



Mineral potential modelling at the British Columbia Geological Survey: Renewed methods with application to northwestern British Columbia

Curran Wearmouth, Thomas A. Czertowicz, Katie J. Peters,
and Evan Orovan



Ministry of
Energy, Mines and
Low Carbon Innovation

Paper 2024-02

Ministry of Energy, Mines and Low Carbon Innovation
Responsible Mining and Competitiveness Division
British Columbia Geological Survey

Recommended citation: Wearmouth, C., Czertowicz, T., Peters, K.J., and Orovan, E., 2024. Mineral potential modelling at the British Columbia Geological Survey: Renewed methods with application to northwestern British Columbia. British Columbia Ministry of Energy, Mines and Low Carbon Innovation, British Columbia Geological Survey Paper 2024-02, 28p.



Ministry of
Energy, Mines and
Low Carbon Innovation



Mineral potential modelling at the British Columbia Geological Survey: Renewed methods with application to northwestern British Columbia

Curran Wearmouth
Thomas A. Czertowicz
Katie J. Peters
Evan Orovan

Ministry of Energy, Mines and Low Carbon Innovation
British Columbia Geological Survey
Paper 2024-02



Mineral potential modelling at the British Columbia Geological Survey: Renewed methods with application to northwestern British Columbia

Curran Wearmouth^{1a}, Thomas A. Czertowicz², Katie J. Peters², and Evan Orovan¹

¹ British Columbia Geological Survey, Ministry of Energy, Mines and Low Carbon Innovation, Victoria, BC, V8W 9N3

² Kenex Pty Ltd Wellington New Zealand, 5013

^a corresponding author: Curran.Wearmouth@gov.bc.ca

Recommended citation: Wearmouth, C., Czertowicz, T., Peters, K.J., and Orovan, E., 2024. Mineral potential modelling at the British Columbia Geological Survey: Renewed methods with application to northwestern British Columbia. British Columbia Ministry of Energy, Mines and Low Carbon Innovation, British Columbia Geological Survey Paper 2024-02, 28p.

Abstract

After about 30 years, The British Columbia Geological Survey is revitalizing its mineral potential mapping efforts. This new modelling takes advantage of information gained from bedrock mapping carried out and mineral occurrences discovered since the 1990s, improved exploration techniques, and a better understanding of the geologic processes leading to mineralization. Furthermore, developments in high-level programming languages and exponential increases in computing power have led to significant advances in applying geographic information system (GIS) platforms and using computerized statistical methods to model mineral potential. The current work adopts a mineral systems approach, which emphasizes similarities between deposits and takes a large-scale view of all the components that control generating and preserving deposits (source, transport, trap, and deposition) using multiple geological features as proxies for the presence of a complete mineral system. We use the weights of evidence method for statistical spatial analysis of many mappable proxies (e.g., distance to intrusive rock contacts, density of fault intersections, presence of anomalous geochemical stream-sediment samples, and occurrence of magnetic high anomalies) to model the mineral potential for porphyry, volcanogenic massive sulphide, and mafic to ultramafic sulphide mineral systems in a large region of northwestern British Columbia. Area-frequency and percentile-frequency plots validate the models and suggest that the region is most prospective for porphyries. The current modelling will assist land-use conversations between multiple parties with diverse interests. The modelling will also be used to evaluate the provincial potential for critical minerals, particularly in underexplored areas.

Keywords: Mineral potential modelling, mineral potential map, land-use planning, mineral systems, statistical methods, geospatial data treatment, predictive maps, weights of evidence, data-driven modelling, porphyry deposits, volcanogenic massive sulphide deposits, magmatic mafic-ultramafic deposits

1. Introduction

The history of British Columbia is intertwined with mining, and the British Columbia Geological Survey has mapped and inventoried the mineral deposits of the province for more than 130 years (Sutherland Brown, 1998). Nonetheless, significant potential for additional discoveries exists because much prospective ground remains underexplored. Land-use decisions and co-management of natural resources require high-quality information and, nearly 30 years ago, the British Columbia Geological Survey initiated a study to assess the mineral potential of the entire province. Applying approaches developed by the United States Geological Survey (Brew, 1992; Singer, 1993) but modified for British Columbia, this work was the first state- or province-wide assessment of its kind. The project combined data about known mineral occurrences and the geology of the province and what was then understood about which rocks favour mineral deposition to develop a relative ranking of mineral potential, with defined 'tracts' of lower to higher potential (Kilby, 1995, 1996, 2004; Grunsky, 1997). Prompted by the global search for critical minerals

needed for a low-carbon future, the Survey started a program to inventory the critical minerals that are produced or could be produced in the province (Hickin et al., 2023, 2024) and renew mineral potential studies with a focus on these minerals. Since the original assessment was carried out, bedrock mapping projects have increased our knowledge of the rocks underlying the province, exploration techniques have improved, many new mineral occurrences have been discovered, and the geologic processes leading to mineralization have been better investigated. Furthermore, developments in high-level programming languages and exponential increases in computing power have led to significant advances in applying geographic information system (GIS) platforms and using computerized statistical methods to model mineral potential (Partington, 2010; Porwal and Kreuzer, 2010; Harris et al., 2015; Kreuzer et al., 2015; Ford et al., 2019; Yousefi et al., 2019, 2021; Ford, 2020; Lawley et al., 2021, 2022). These advances have been adopted by geoscientists in industry, government, and academia for appraising mineral potential (Knox-Robinson and Wyborn, 1997; Harris et al., 2015; Kreuzer et al., 2015;

Lawley et al., 2021, 2022; McCafferty et al., 2023; Nykanen et al., 2023). The rejuvenated modelling at the British Columbia Survey applies the weights of evidence modelling technique, which, although is three decades old, has benefited from these advancements.

In this paper we focus on the methods we used to consider the prospectivity of porphyry, volcanogenic massive sulphide, and magmatic mafic to ultramafic sulphide deposits for a large region of northwestern British Columbia (Fig. 1), the results of which are presented in a series of mineral potential maps (Wearmouth et al., 2024a). A comparison of results between work done in the 1990s and a version of the current modelling is given by Wearmouth et al. (2024b). Elsewhere, Wearmouth

et al. (2024c) present results for the sedimentary exhalative (SEDEX) and Mississippi Valley-type mineral systems in a large area of northeastern British Columbia.

The current study area includes the lands and traditional territories of many Indigenous rights holders, and this new mineral potential modelling will support decision-making processes and land-use decisions. The new work will also be used to evaluate the potential for critical minerals in the province, which are needed to support the low-carbon transition, grow the economy, diversify global supply chains, and continue as a preferred supplier for partner nations (Hickin et al., 2023, 2024).

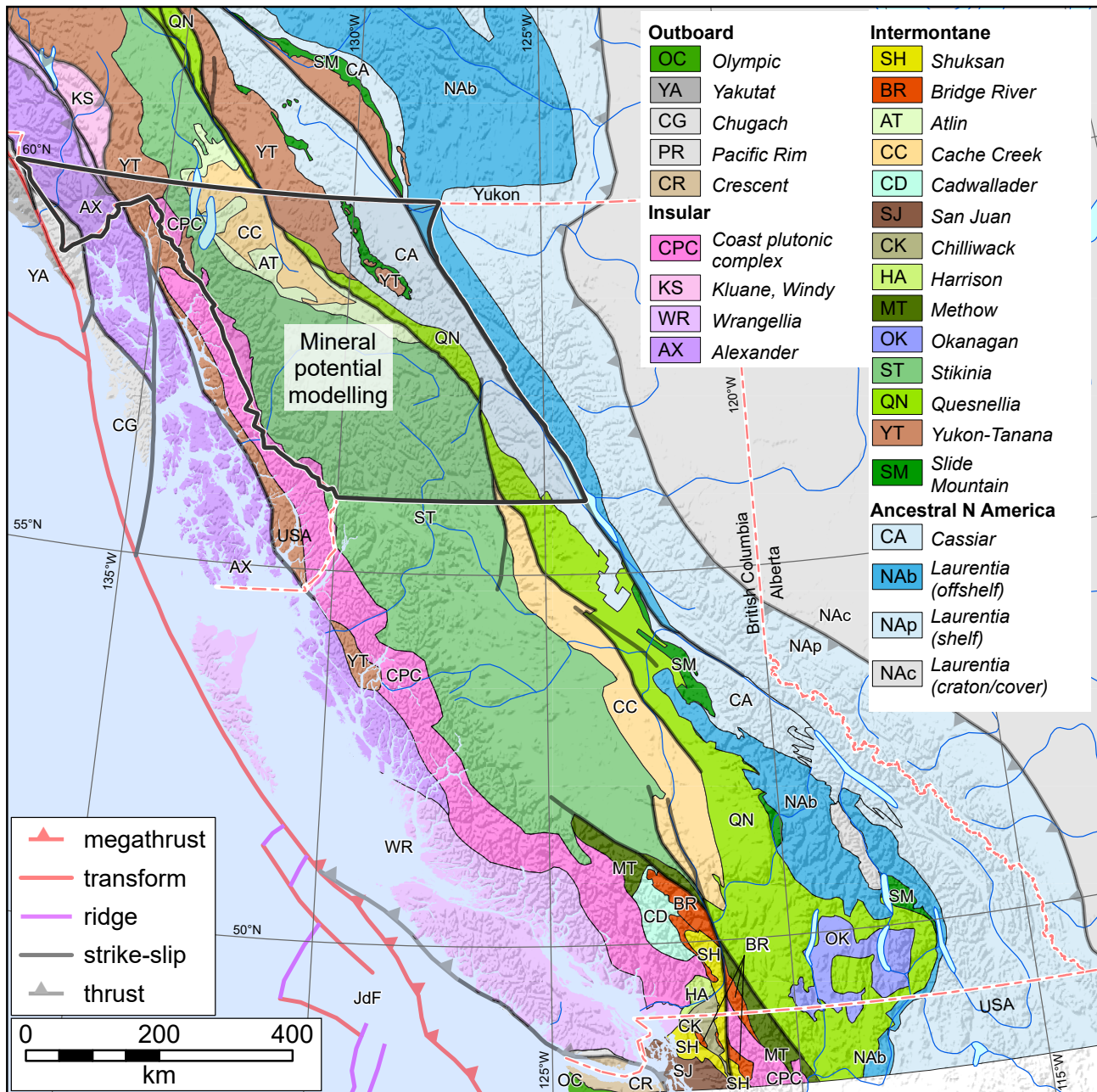


Fig. 1. Mineral potential modelling study area, 2023. Terranes after Colpron (2020).

2. Methods

2.1. Modelling techniques

Depending on the purpose and the data available, different methods can be used to assess the mineral potential of an area. These methods are commonly expressed in terms of being ‘knowledge-driven’ (‘expert-driven’) or ‘data driven’ (e.g., Bonham-Carter, 1994, p. 269). However, these terms are pure end members of a continuum and are unlikely to fully apply to any given case. For example, even though the 1990s BCGS modelling relied heavily on geoscience experts to make key decisions, it was based on the same data sources as the current work. The current work benefits from the knowledge gained from updates to these sources. Similarly, even though the current modelling uses computer algorithms instead of geoscience experts, human interventions and expert knowledge are still required at different stages. The fundamental difference between knowledge-driven and data-driven modelling is in how weights are assigned to the data (Bonham-Carter, 1994). In knowledge-driven methods, data are reviewed and subjectively weighted by experts, relying on their level of expertise, and are thus considered more subjective (Bonham-Carter, 1994). Examples of knowledge-driven techniques include index overlay (Yousefi and Carranza, 2016) and fuzzy logic (e.g., Porwal et al., 2003). In data-driven methods, computer algorithms seek statistical associations or patterns within data to determine relevance to known training data and are thus considered more objective. Examples of data-driven methods include weights of evidence (e.g., Bonham-Carter et al., 1990), random forest (Ford, 2020), and neural networks (Singer and Kouda, 1999).

Any approach to modelling is limited by the data available, and results represent a time-specific evaluation; as new discoveries are made or additional data collected, older modelling may need updating (Ford et al., 2019). Knowledge-driven methods require no training data and may be more effective in underexplored or data-poor areas. Because of advances in GIS applications and computer power, statistical analysis of multivariant spatial data using ‘data-driven’ methods is far less labour intensive than the ‘knowledge-driven’ work done by the Survey in the 1990s, can be readily updated, and is more easily reproducible. We applied weights of evidence modelling as the data-driven method in this study.

Weights of evidence is a Bayesian statistical approach that allows the analysis and combination of various datasets to predict the location of a feature (Bonham-Carter, 1994). This technique calculates the relationship of the feature being tested for a given area and the number of training data points, in this case sites of mineralization, that fall within that area. The statistical spatial analysis process allows for a non-biased assessment of many mappable proxies (e.g., distance to intrusive rock contacts, density of fault intersections, presence of anomalous geochemical stream-sediment samples, and occurrence of magnetic high anomalies) for ore-forming processes to determine their relevance to the mineral system (Bonham-Carter, 1994). We used the Arc-SDM extension for ArcGIS to carry out this analysis and the mineral potential modelling.

2.2. Mineral systems approach

Although mineral occurrences are relatively common, mineral deposits of economic value are not. All the right geological conditions need to come together at the right time and in the right place for an economic deposit to form. The mineral potential work carried out by the Survey in the 1990s (e.g., Kilby, 2004) emphasized the differences between deposit types and focussed on deposit profiles that classified occurrences into about 120 deposit types based mainly on genetic models (e.g., Lefebvre and Jones, 2022). These profiles included descriptions of geological characteristics, mineral exploration techniques, resource data, age of mineralization, tectonic setting, and concepts about deposit origins.

In contrast, the current assessment adopts a mineral system approach, which emphasizes similarities between deposits and uses a large-scale view of all the factors that control generating and preserving deposits (e.g., Knox-Robinson and Wyborn, 1997; Hronsky and Groves, 2008; McCuaig et al., 2010; Ford et al., 2019; Groves et al., 2022). Originally proposed by Wyborn et al. (1994) and drawing on ideas from the petroleum industry (e.g., Magoon and Dow, 1994), the geological components that have been traditionally used to define a single mineral system include energy to drive the system, source of ligands, source of metals, transport pathways, traps, and outflow zones (Knox-Robinson and Wyborn, 1997). Adapting the traditional use, the mineral system concept that we adopt uses source, transport, and trap, as well as deposition of mineralization to consider the presence of a complete mineral system. The approach recognizes that the ore deposit, which is relatively small (<1 km in plan view), is the central feature of a larger system that may be detectable at a regional scale (>10 km in plan view). The mineral systems approach focusses on processes that are common within mineral systems, which enables the simultaneous assessment of many deposit types at a variety of scales (McCuaig et al., 2010). An economic deposit is unlikely if any one of source, transport, and trap are lacking; areas that bear evidence for all components will be evaluated as being favorable for mineralization. Being process-based, the mineral systems approach is neither restricted to a geological setting nor limited to a specific ore deposit type.

2.3. Mineral potential modelling workflow overview

The current mineral potential modelling workflow (Fig. 2), based on Agterberg et al. (1990), Bonham-Carter et al. (1990), Knox-Robinson and Wyborn, (1997), and Harris and Sanborn-Barrie (2006), uses multiple datasets, knowledge of mineral systems, and the weights of evidence (WofE) technique to assess mineral potential. At the start of a project, a study area is reviewed for known mineralization or known ore deposit types, which are used to define the mineral systems in the region and to identify training points. The targeted mineral systems are then broken down into the critical processes that dictate their formation, and a list of predictive variables is developed. Available data are then interrogated for mappable features that may represent one or more of these formative processes. At this stage, data processing may be required such as classifying,

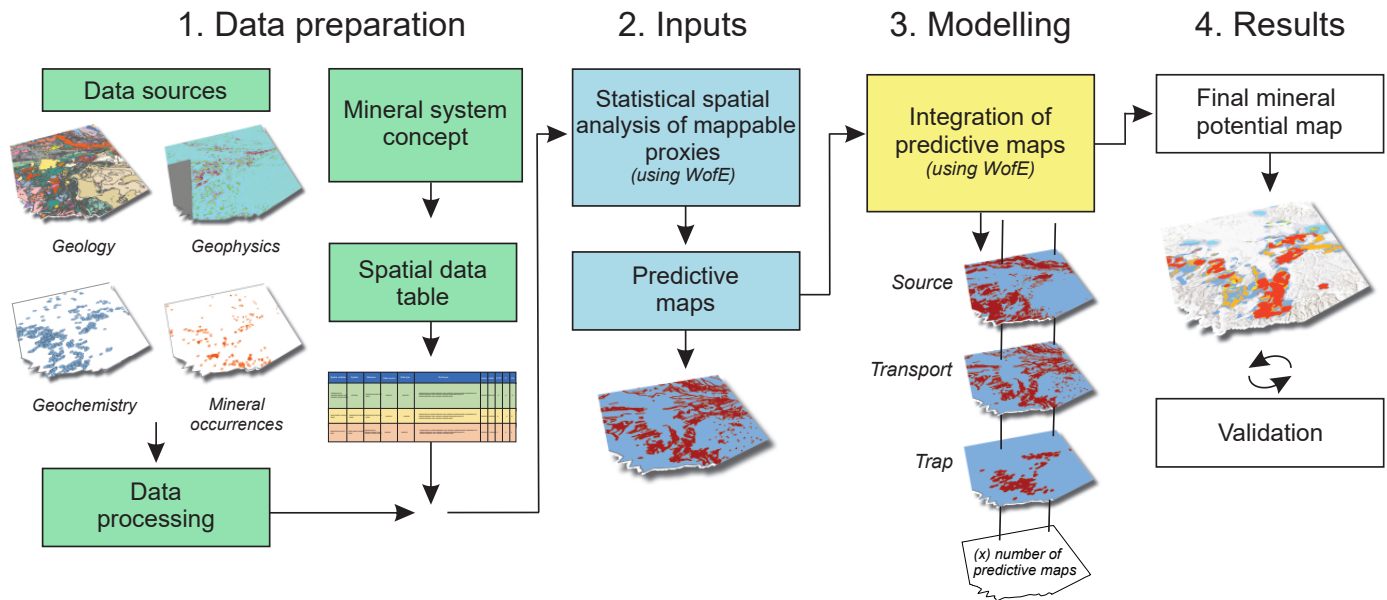


Fig. 2. Simplified workflow of the mineral potential modelling process. 1) Data preparation: multiple datasets are collected and processed. The mineral system of interest is broken down into the critical ore-forming processes and a list of predictive maps is produced in the form of a spatial data table. 2) Inputs: processed data are tested for statistical correlation with known mineralization in the study area using the weights of evidence (WofE) method and predictive maps are generated. 3) Modelling: a selection of predictive maps is then chosen to be integrated into a final mineral potential map. 4) Results: final mineral potential maps are validated with known mineralization in the study area.

interpolating, filtering, and attributing raw data. Using the weights of evidence method, statistical spatial analysis is conducted on raw or processed data to determine its relevance to training points, which represent known mineralization in the study area. This process results in the creation of predictive maps (binary or multi-class), which represent map patterns that, based on the statistical correlations, are deemed to be potential predictors for the mineral system. Each predictive map is given a weighting based on its spatial association with the training points, which is calculated using the weights of evidence technique (Bonham-Carter et al., 1990; Bonham-Carter, 1994).

Although the weights of evidence modelling technique is primarily data driven, expert knowledge and input are needed at several stages of the workflow to ensure that the results are geologically meaningful. For example, a selection of predictive maps, which typically have the highest spatial correlation with the training points, are chosen by a geologist to be integrated using weights of evidence. The final mineral potential map illustrates the relative geologic potential for the mineral system across the study area. Final models may also be validated using other known mineral occurrences in the study area that were not used in the modelling process (Bonham-Carter et al., 1990; Bonham-Carter, 1994).

Whereas other data-driven modelling techniques have demonstrated greater predictive performance, weights of evidence benefits from its ease of interpretability and handling of missing values. Weights of evidence provides a clear and interpretable framework, which is crucial to understand the reasoning behind predictions. Machine learning modelling methods such as neural networks commonly act as ‘black boxes’, making it challenging to identify how the input maps

affect the prospectivity values. Readily explainable results are important in cases, such as land-used planning, where different parties faced with making decisions that have long-term consequences have a common understanding (Samek and Müller, 2019). Furthermore, weights of evidence can explicitly manage missing values during the modelling process without the need for imputation. The areas of missing data are assigned a neutral weight to account for these areas in the statistical calculations (Ford, 2015). In comparison, machine learning models require data to be imputed for these areas, which may not account for the complexity, variability, and spatial correlation inherent in many geological datasets.

3. Northwestern British Columbia study

3.1. Study area

In this study, we focus on arc-related terranes in northern British Columbia (north of latitude 56°) that are prospective for the porphyry, volcanogenic massive sulphide, and magmatic mafic to ultramafic sulphide mineral systems, eliminating areas east of the Rocky Mountain trench, which lack these systems.

3.2. Geologic context

The study area spans a large segment in the northwestern part of the Canadian Cordillera (Fig. 1). This 2000 km long northwest-trending accretionary orogen consists of several long, narrow, far-travelled ‘exotic’ terranes (in some cases, 1000s of km) that welded to the western margin of Ancestral North America in the last 180 million years (e.g., Nelson et al., 2013; Colpron and Nelson, 2021). The Cordillera records a history of supercontinent rifting and a succession of island arc volcanosedimentary and intrusive assemblages (terranes) developed outboard of

Ancestral North America and accreted to each other and to the proto-continental margin with final amalgamation produced by collisions driven by westward motion of the North American continental plate. The amalgamated Cordillera then became the site of Cretaceous and Cenozoic arc and post-arc magmatism. Terrane evolution continues today as the Juan de Fuca plate slides beneath Vancouver Island. As reviewed by Nelson et al. (2013), Hickin et al. (2017) and Colpron and Nelson (2021), the diverse tectonic processes, from supercontinent breakup through development of long-lived arc terranes, to terrane accretion and post-accretion magmatism, metamorphism, deformation, and sedimentation, have generated diverse mineral systems across the province.

West of Ancestral North America, Cordilleran terranes are commonly grouped into superterranes and terranes (Fig. 1). In Ancestral North America (including Cassiar terrane), predominantly sedimentary rocks were deposited on Archean and Paleoproterozoic cratonic basement. These Paleoproterozoic to Cambrian successions were deposited during and after the breakup of the supercontinent Rodinia, which created the western margin of Laurentia, the nucleus of what is now North America. The Intermontane superterrane consists of a diverse group of Late Paleozoic to Mesozoic volcanosedimentary assemblages and kindred intrusive bodies that formed mainly in and adjacent to island arcs outboard of Ancestral North America in the proto-Pacific Ocean. The Insular superterrane consists of similar island arc terranes; the Intermontane-Insular terrane boundary lies within the syn- to post-accretionary Coast Plutonic complex, a linear arc-axial belt that extends the length of the Cordillera. The Outboard terranes are mostly late Mesozoic to Cenozoic forearc siliciclastic assemblages, bounded to the west by the present-day Cascadia subduction zone and Queen Charlotte fault. Modern-day volcanic complexes related to Cascadia subduction are distributed along the length of the western Cordillera, and many of the terranes are partially covered by sedimentary rocks that were deposited during terrane accretion and collision, when older rocks were deformed, uplifted, eroded, and redeposited in newly created sedimentary basins.

Current exploration in the study area, which includes parts of the Northwest and North Central mining regions, focuses on a diverse suite of deposits (see summary in Clarke et al., 2024). The study area includes two active mines (Brucejack and Red Chris) and one mine (Premier Gold) is on track to have its first gold pour in 2024. All three are in the ‘Golden Triangle’, the popular name for a loosely defined area in the Northwest Region containing significant gold, silver, copper, and molybdenum deposits (British Columbia Geological Survey, 2023).

3.3. Mappable mineral system proxies

The source, transport, trap, and deposition processes of mineral systems may be represented spatially using geological proxies (Ford et al., 2019). To produce such proxies, research into the mineral system, both generally and specific to the region

being modelled, is undertaken at the beginning of a project. Information can come from a variety of sources including in-house expertise, company reports, and the literature. This information is used to prepare a list of all the ore-forming processes that describe the mineral system (McCuaig et al., 2010; Ford et al., 2019) that can serve as mappable proxies to be tested in the modelling process. The modelling work presented herein considers the porphyry, volcanogenic massive sulphide, and magmatic mafic to ultramafic mineral systems.

3.3.1. Porphyry mineral systems

Porphyry systems can form low-grade (commonly <0.5%), high-tonnage (commonly > 100 Mt) ore bodies where silica-rich magmas migrate upwards to solidify at shallow levels in the Earth’s crust and are chemically altered by circulating hot waters. They form in subduction settings where hydrous arc magmas generated by partial melting of the down going slab and adjacent mantle scavenge metals and rise into the overlying crust (e.g., Sillitoe, 1972, 2010; Lee and Tang, 2020; Rezeau and Jagoutz, 2020; Park et al., 2021). Episodes of porphyry copper, molybdenum, gold, and silver mineralization, particularly in the 15 million-year interval spanning the Jurassic-Triassic boundary in Quesnellia and Stikinia (Fig. 1), are important to British Columbia as a whole (Logan and Schroeter, 2013; Logan and Mihalynuk, 2014; Sharman et al., 2020) and in our study area (e.g., Rees et al., 2015; Febbo et al., 2019; Nelson and Van Straaten, 2020; Ootes et al., 2020; Ootes, 2023; van Straaten et al., 2023). In addition to the current Red Chris mine, the study area contains numerous porphyry related past-producing mines, current proposed mines, and advanced exploration projects (Clarke et al., 2024), the generation of which is directly tied to the multistage evolution of the Stikine and Quesnel arc terranes between ca 220 and 170 million years ago (Nelson and Van Straaten, 2020). Of the 11 mines that operated in British Columbia in 2023, seven are porphyry deposits, and the province is the largest Canadian producer of copper and only producer of molybdenum, both of which are on the national critical minerals list (NRCan, 2022). They may also contain other minor ‘companion metals’ (Mudd et al., 2017) such as the platinum group elements (PGE), rhenium, tellurium, and, in the more Mo-rich porphyry deposits, beryllium, bismuth, lithium, niobium, the rare earth elements, tantalum, tin, and tungsten (Sillitoe 1983; Nobel et al., 1995; John and Taylor 2016; Mihalynuk and Heaman, 2002; Velasquez et al., 2020).

3.3.2. Volcanogenic massive sulphide mineral system

Volcanogenic massive sulphide (VMS) deposits are accumulations of sulphide minerals precipitated at sites of rift-related submarine volcanism on the floors of ancient and modern seas. The deposits form where metal-rich fluids heated by volcanic processes rise, discharge, and mix with seawater (Lydon, 1984, 1988; Franklin et al., 2005; Galley et al., 2007; Cousens and Piercey, 2008; Piercey, 2011, 2015; Ross and Mercier-Langevin, 2014), and may contain economic

concentrations of copper, zinc, lead, silver, gold, and cobalt. Different types of VMS deposits are distributed across the study area in the Cache Creek, Yukon-Tanana, and Alexander terranes and, particularly, near the western flank of Stikine terrane, which hosts several past-producing mines (Barresi et al., 2015; Nelson and Van Straaten, 2020; Hunter et al., 2022; Northcote, 2022). The primary metals are copper and zinc, with secondary lead. More rarely, volcanogenic massive sulphide systems contain cobalt (e.g., Windy-Craggy, Peter and Scott, 1999; Leybourne et al., 2022), or are rich in gold and silver (Eskay Creek; Sherlock et al., 1999; Mercier-Langevin et al., 2011). Potential companion critical metals include bismuth, cobalt, gallium, germanium, indium, antimony, tin, tellurium, and thallium (Paradis, 2015; Leybourne et al., 2022).

3.3.3. Magmatic mafic to ultramafic mineral system

Magmatic mafic to ultramafic sulphide deposits, commonly with concentrations of nickel, copper, platinum group elements, and chromium, are found in mafic to ultramafic intrusive bodies where sulphide minerals have crystallized and settled in magma chambers sourced from mantle-derived melts (Naldrett, 1999, 2010; Barnes and Lightfoot, 2005; Lawley et al., 2021). Although commonly considered to be related to rifts and/or plumes at sites of plate divergence, deposits formed at sites of plate convergence in suprasubduction, or post-subduction settings are being increasingly recognized. These include deposits in the Yukon-Tanana and Quesnel terranes of the study area that were emplaced during accretion of arc terranes to Ancestral North America (Nixon et al., 2019, 2020; Nott et al., 2019). Magmatic mafic to ultramafic sulphide deposits represent a significant system that may host economic concentrations of nickel, copper, the platinum group elements and may have companion metals such as vanadium, titanium, chromium, and scandium (Wang et al., 2021).

3.4. Geospatial data sources

The data used in the current modelling come from MINFILE, BC Digital Geology, and geochemical databases curated by the British Columbia Geological Survey and integrated with MapPlace, the Survey's open access geospatial web service. We also used regional-scale gravity (NRCAN, 2020a) and aeromagnetic data (NRCAN, 2020b). MINFILE is an inventory documenting more than 16,100 metallic mineral, industrial mineral, and coal occurrences in the province. It provides information about occurrence location, host rock, mineralogy, commodities, country rocks, cross-cutting intrusions, structures, metamorphism, alteration, age, presumed deposit type, and grade and tonnage. BC Digital Geology provides bedrock geology mapping with a typical scale of 1:50,000 (Cui et al., 2017). The provincial geochemical databases hold field and geochemical data from multi-media surveys by the Geological Survey of Canada, the BCGS, and Geoscience BC. The databases contain results from the Regional Geochemical Survey program including analyses from stream-sediment, lake sediment, moss, and water samples (e.g., Lett, 2011;

Hickin and Plouffe, 2017; Lett and Rukhlov, 2017; Han and Rukhlov, 2020a), till surveys (Bustard et al., 2017, 2019), and lithochemical samples (Han and Rukhlov, 2020b). We chose datasets that had maximal spatial coverage across the study area and the ability of the data to capture the components of a mineral system unambiguously.

3.5 Geospatial data processing

Compiled data were processed by classifying and attributing rock units, creating point datasets from fault data (fault intersections, bends, jogs, and splays), generating stream catchment maps and, for geochemical data, determining anomalous thresholds and creating geochemical anomaly grids.

Bedrock geology was queried into groupings such as rock type, terrane designation, lithostratigraphic unit, interpreted environment, and specific time interval (for a complete description of rock groupings for each mineral system see Appendix A, [BCGS_P2024-02.zip](#)). Fault data were concatenated by joining contiguous line segments with similar orientations. Faults lengths and average orientations were then attributed to the concatenated lines. Derivative point datasets were produced from fault polylines that represent intersections, bends, jogs, and splays. These datasets were created using data processing tools in MapInfo spatial data modelling software (MI-SDM). Fault intersections were defined as points where faults cross or touch, regardless of their orientation. Fault bends were defined as any change in angle of between 15 and 80 degrees along a fault length of 0 to 10 km. Fault jogs were defined as any two connected subparallel fault segments (<30° difference in angle) with an overlap or underlap of up to 500 m and a separation between the segments of 100-300 m. Fault splays were defined as nodes between a primary fault and another fault segment branching off at an angle of 5-35°, with a maximum separation of 100 m between the two segments and a minimum distance of 100 m from the end of the primary fault.

Geochemical datasets were reviewed to ensure that the range of reported values was reasonable for each element. In cases of analysis by different methods, results from the most precise modern technique were used. Below detection results were replaced with half of the lowest detection limit for each element. Anomalous thresholds were determined for each element from stream sediment and lithochemical samples using whole dataset statistics. The thresholds (Table 1) were determined by examining the percentile values, cumulative probability plots, and Tukey Outliers (defined as 1.5 multiplied by the inter-quartile range). Using the anomalous thresholds as cutoffs, the geochemical point data were rasterized into grids. Areas above the threshold value were considered anomalous, areas below the threshold were non-anomalous; no-data areas were also included in the weights of evidence calculations. Lithochemical data (n=3,575), collected as bedrock grab samples, were converted into maps for each element by buffering to 2000 m, attributing each buffered polygon as anomalous, non-anomalous, or no data (no sample or element not measured), and converted into a raster, while giving

Table 1. Geochemistry anomalous threshold values.

Stream sediment (in ppm)

Element	Threshold	Tukey Outlier	Probability plot	75 th Percentile	85 th Percentile	95 th Percentile
Ag	0.33	0.33	0.40	0.17	0.28	0.46
As	23	23	28	11	18	38
Au	0.010	0.010	0.011	0.004	0.008	0.022
Co	33	33	29	18	22	30
Cr	134	134	130	65	94	169
Cu	106	106	111	54	74	110
Mo	4	4	8	2	4	7
Ni	121	121	115	58	91	142
Pb	19	19	17	10	14	26

Litho-geochemistry (in ppm unless otherwise stated)

Element	Threshold	Tukey Outlier	Probability plot	75 th Percentile	85 th Percentile	95 th Percentile
Ag	2.4	2.4	1.1	1.0	5.0	43.0
Au	67	67	61	27	140	1261
Co	103	103	86	46	83	190
Cr	202	202	230	86	205	458
Cu	235	419	235	177	1005	9500
Ni	95	95	180	40	84	390
Pb	42	42	67	19	46	938
S (%)	0.3	0.3	0.4	0.1	0.7	2.5
Zn	223	223	129	113	204	2230

priority to the anomalous polygons where they overlap with non-anomalous or no data areas.

Stream geochemical data (n=14,834) were analyzed using a digital elevation model (DEM) image to define catchments with hydrology tools in MapInfo Discover. One map was created for each element by determining the catchments that contain anomalous samples and the catchments that only contain non-anomalous samples, and then combining the two to create a multiclass grid (including catchments with no data as the third class). An alternative approach was also tested in which we averaged the stream sediment assays within each catchment and then reclassified the resulting raster into ten classes, which were then tested for spatial association.

3.6. Training points

The weights of evidence method requires sites of known mineralization to use as training points for determining spatial correlations and weights for each predictive map being tested. We selected training points for the three mineral systems from the MINFILE database based on spatial distribution, representation of the mineral system, and the degree of confidence in the interpreted mineral system classification. To avoid including erroneous classified training data, the number of training points was limited to known, well-studied deposits positively identified as being representative of a given mineral system. The porphyry model has twelve training points (Table

2, Fig. 3), the VMS model has eleven (Table 3, Fig. 4), and the magmatic mafic to ultramafic sulphide model has eight (Table 4, Fig. 5); Appendix B ([BCGS_P2024-02.zip](#)).

3.7. Spatial analysis using weights of evidence

The study area was converted into a 50 m by 50 m grid, which was chosen as the minimum scale that the data could be viewed and used. The cell size represents the resolution of the model and the cell distribution for all subsequent grids created during the modelling process. A training point representing an economic deposit was presumed to have an average footprint of 1 km². This assumed footprint, referred to as a unit cell area, was used in the weights of evidence calculations for each training point.

Applying the weights of evidence method as described by Bonham-Carter et al. (1990) and Bonham-Carter (1994) and using input parameters (area being examined, unit cell area, number of training points) a 'prior probability' was calculated for each mineral system (Appendix A, [BCGS_P2024-02.zip](#)). This prior probability represents the chance of randomly discovering a deposit before any additional evidence for mineralization is applied. The aim of weights of evidence modelling is to test if adding evidence increases or decreases the value of the prior probability of each grid cell. The probability of finding a new occurrence after adding layers of evidence is referred to as the 'posterior probability'. In the present example, factors

Wearmouth, Czertowicz, Peters, Orovan

Table 2. Porphyry model training points.

Name	Status	Mineralization style	Cordilleran belt	Terrane
Galore Creek	Developed prospect	Alkalic porphyry Cu-Au	Intermontane	Stikine
Kemess South	Past producer	Porphyry Cu +/- Mo +/- Au	Intermontane	Stikine
Schaft Creek	Developed prospect	Porphyry Cu +/- Mo +/- Au	Intermontane	Stikine
Saddle North	Prospect	Porphyry Cu +/- Mo +/- Au,	Intermontane	Stikine
Mitchel	Developed prospect	Porphyry Cu +/- Mo +/- Au	Intermontane	Stikine
Red Chris	Producer	Porphyry Cu +/- Mo +/- Au,	Intermontane	Stikine
Thorn	Prospect	Subvolcanic Cu-Ag-Au (As-	Insular	Stikine
Eaglehead	Developed prospect	Porphyry Cu +/- Mo +/- Au	Intermontane	Quesnel
Bronson Slope	Developed prospect	Porphyry Cu +/- Mo +/- Au,	Insular	Stikine
Gnat Pass	Developed prospect	Porphyry Cu +/- Mo +/- Au	Intermontane	Stikine
Hat	Prospect	Alkalic porphyry Cu-Au	Intermontane	Stikine
Ruby Creek	Developed prospect	Porphyry Mo (Low F- type)	Intermontane	Cache Creek

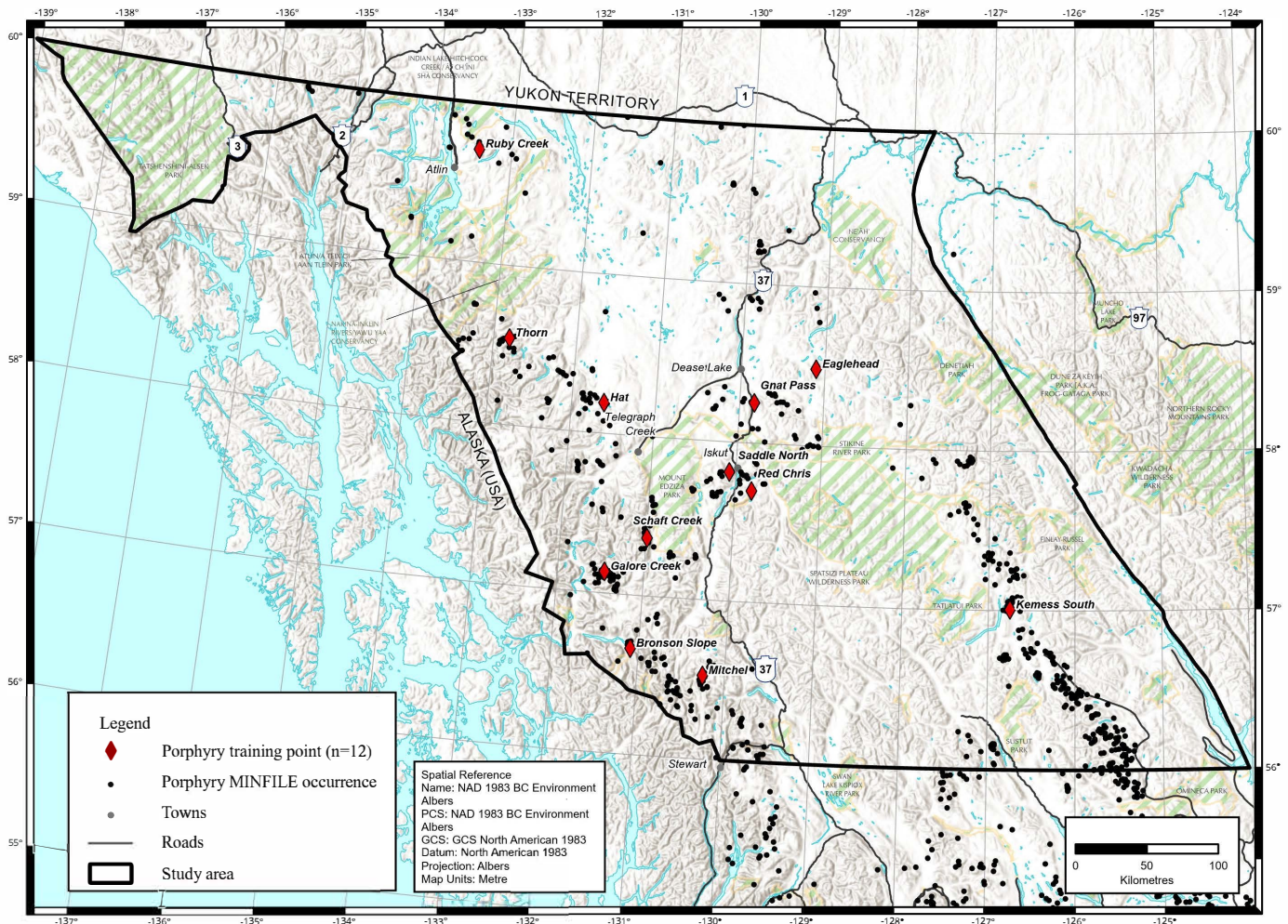


Fig. 3. Training points used in the porphyry model (red diamonds) and all porphyry mineral occurrences (black dots). Data from MINFILE.

Wearmouth, Czertowicz, Peters, Orovan

Table 3. Volcanogenic massive sulphide model training points.

Name	Status	Mineralization style	Cordilleran belt	Terrane
Eskay Creek	Past producer	Noranda/Kuroko	Intermontane	Stikine
Dago	Past producer	Noranda/Kuroko	Intermontane	Stikine
Tulsequah Chief	Past producer	Noranda/Kuroko	Intermontane	Stikine
Kutcho	Developed prospect	Noranda/Kuroko	Intermontane	Quesnel
Granduc	Past producer	Besshi	Intermontane	Stikine
Rock and Roll	Developed prospect	Besshi	Intermontane	Stikine
Joss'alun	Prospect	Cyprus	Intermontane	Stikine
Windy Craggy	Developed prospect	Besshi	Insular	Alexander
Mount Henry Clay	Prospect	Besshi	Insular	Alexander
Foremore	Prospect	Noranda/Kuroko	Intermontane	Stikine
Inel	Developed prospect	Besshi	Intermontane	Stikine

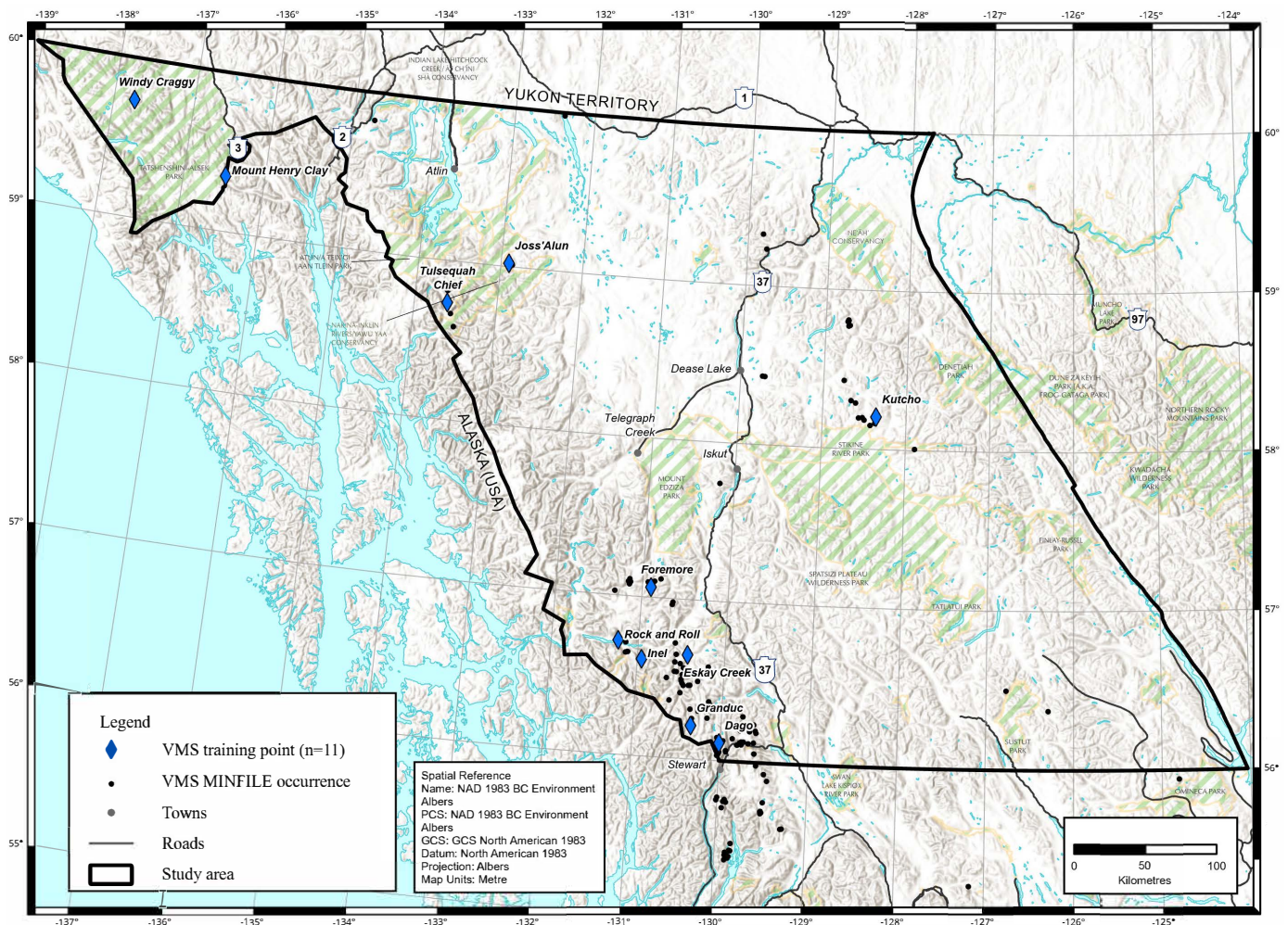


Fig. 4. Training points used in the volcanogenic massive sulphide model (blue diamonds) and all volcanic massive sulphide mineral occurrences (black dots). Data from MINFILE.

Table 4. Magmatic mafic-ultramafic model training points.

Name	Status	Mineralization style	Cordilleran belt	Terrane
E&L	Developed prospect	Tholeiitic intrusion-hosted	Intermontane	Stikine
Turnagain Nickel	Developed prospect	Alaskan-type	Intermontane	Yukon-Tanana
Orca	Showing	Alaskan-type	Intermontane	Cache Creek
Nixon	Showing	Alaskan-type	Intermontane	Quesnel
Queen	Prospect	Alaskan-type	Intermontane	Quesnel
Anyox-Rodeo	Showing	Mafic-ultramafic associated	Intermontane	Stikine
Taurus	Showing	Alaskan-type	Intermontane	Quesnel
TNS12	Showing	Tholeiitic intrusion-hosted	Intermontane	Stikine

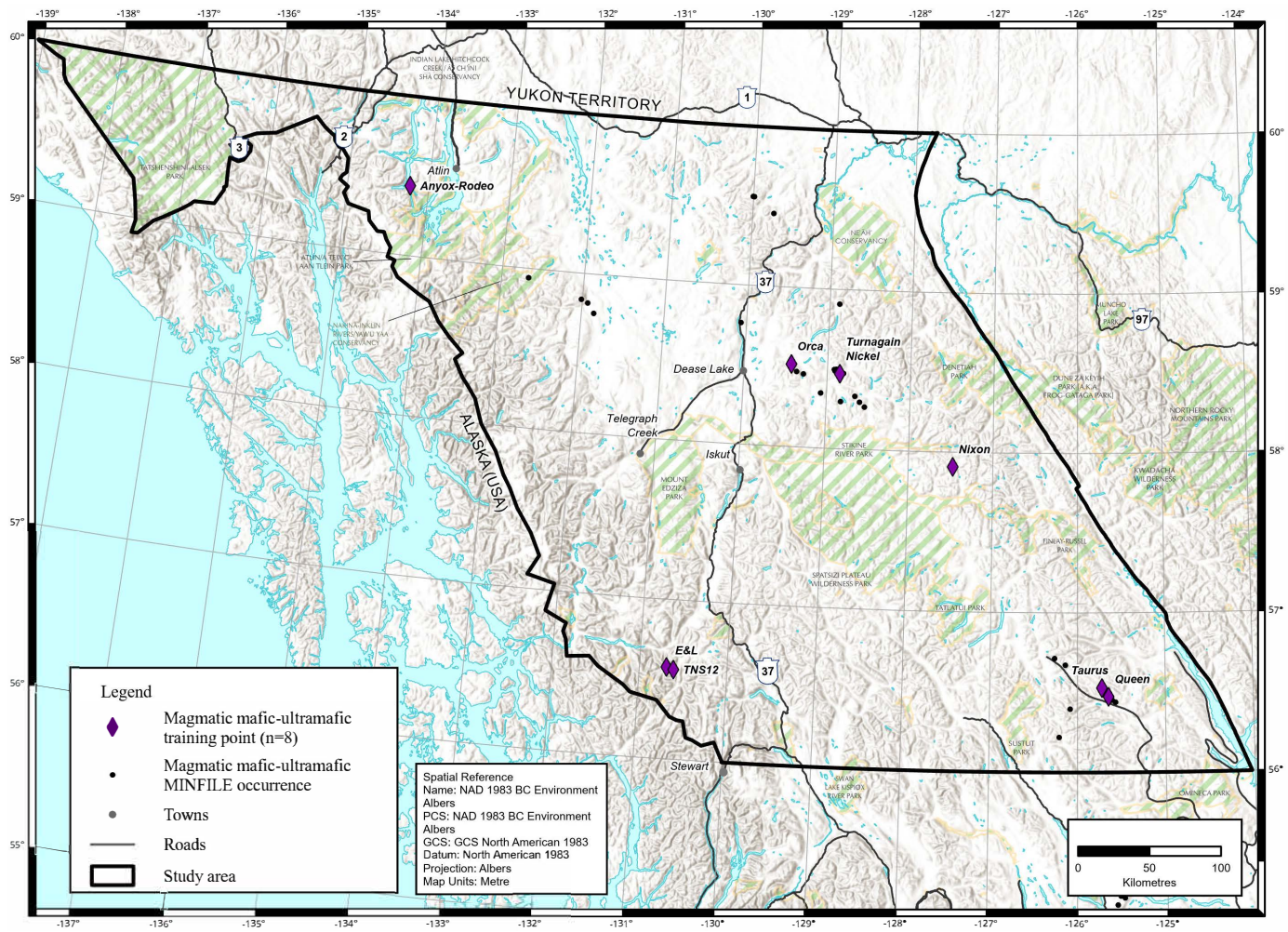


Fig. 5. Training points used in the magmatic mafic to ultramafic sulphide model (purple diamonds) and all mafic-ultramafic sulphide mineral occurrences (black dots). Data from MINFILE.

that lead to posterior probability values that are greater than prior probability values were layered into the mineral potential model. Layers of evidence, or predictive maps, that reduce the search space while capturing the most training points will have the best spatial correlations and their combination will result in highest posterior probabilities when combined into the model (Bonham-Carter, 1994; Bonham-Carter et al., 1990).

The spatial correlation of a mappable feature (e.g., distance to faults) is calculated by using the relationship between the area including the feature and the number of training points within that area compared to the number of points outside. In the presence of a feature, the calculation produces a positive W^+ value for features that correlate with the training data and a negative W^- value for the features that do not correlate. In the absence of a feature, the opposite applies for the W^- value. Each feature gets a W^+ and a W^- value representing its positive and negative weight. These values are the weights that are used in the model calculations when the predictive maps are combined into a mineral potential map (Bonham-Carter et al., 1990; Bonham-Carter, 1994).

The spatial correlation (contrast value 'C') is calculated from the difference between W^+ and W^- . The standard deviations of W and C (W_s and C_s) are also calculated. These values are used to calculate studentized value of the contrast (StudC) which is the ratio of the standard deviation of the contrast (C_s) to the contrast (C). This provides an indication of the uncertainty in the C value; if the contrast is large compared with its standard deviation, it implies that the contrast is more likely to be real. The higher the values of C and StudC the stronger the spatial correlation of the feature being tested with the training data (Bonham-Carter et al., 1990; Bonham-Carter, 1994).

4. Spatial correlation results

The mappable proxies that represent one or more of the ore-forming processes for a particular mineral system are used to create predictive maps. Statistical spatial analysis using the weights of evidence method, as described above, is applied to a list of such proxies to create binary or multi-class predictive maps, and to derive weights that are used to combine the predictive maps into the final mineral potential map (Appendix B, [BCGS_P2024-02.zip](#)).

First, mappable proxies are tested for spatial correlation with the training data. Polygon features such as geological units can be tested directly for statistical significance based on the presence of a feature, or by buffering a feature at varying distances to identify an area of influence such as ground surrounding an intrusion, or to account for shallowly dipping units or uncertainty in the mapping. Point and line data are typically buffered to multiple distances before being tested. These data can also be gridded to determine the density of features or to show the interpolated distribution of elements, such as for a geochemistry dataset. Continuous data like geophysics maps or density grids, are reclassified into a small number of groups to test for correlation with training data.

The spatial correlation results from the tested features are

used to determine how the data are classified into binary maps based on the statistical results and geological reasoning. For example, when testing multiple distance buffers to determine the optimal distance from a feature (e.g., proximity to faults) the C value (as described above) can be used to determine the cutoff distance (Fig. 6). However, because there isn't always a clear maximum on the contrast curve, subjective judgment, supported by geological reasoning, comes into play (Bonham-Carter, 1994). If the cutoff distance is geologically unreasonable, a geologically reasonable distance with a lower C value, but still statistically valid, needs to be used.

This statistical spatial analysis is repeated for different data sets to create a list of predictive maps that collectively represent the mineral potential for a mineral system. The predictive maps

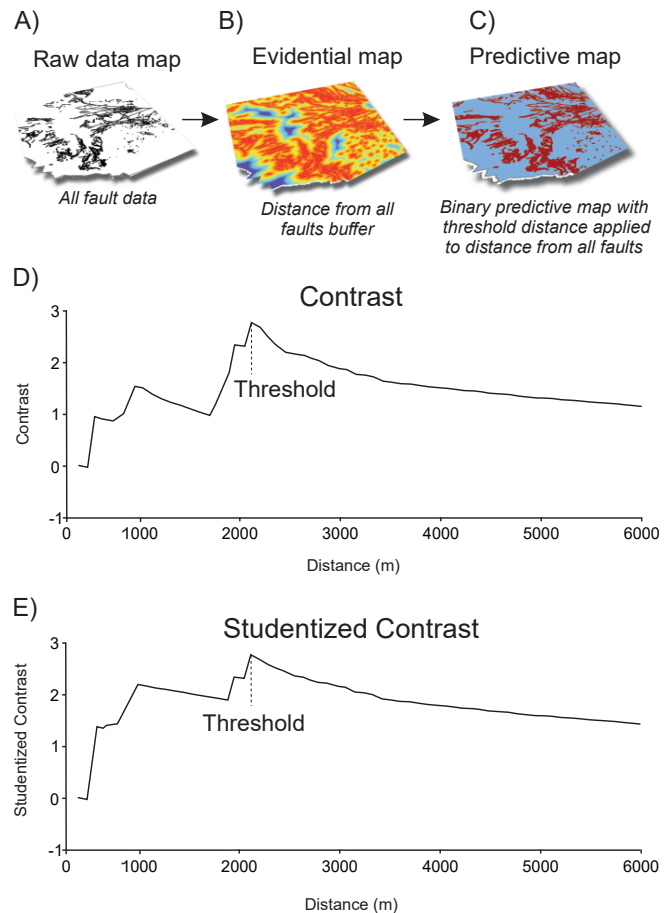


Fig. 6. Testing multiple buffer distances to determine the optimal distance. **a)** Proximity to fault map is used as the original feature. **b)** Buffer distance applied to fault traces. Contrast values are calculated for every 50 m from fault traces. **c)** The area inside the determined cutoff distance (red) will be classified as favourable to create a binary predictive map, and everything outside (blue) will be classified as unfavourable. **d)** Contrast value plot vs distance from fault trace. The highest contrast value (near 2200 m) indicates the highest statistical correlation with the training data and the area captured by the buffer is greatest at 2200 m. **e)** Studentized contrast plot vs distance from fault trace. The higher the studentized contrast value the more likely the value is valid, which in this case corresponds to 2200 m from the fault trace.

are typically binary (feature present/feature absent) but can also be multiclass, such as in the case of fault density where it may be relevant to define areas of low, moderate, and high density in the same map. The weights for the final predictive maps are recalculated to integrate into the final model. The spatial analysis we used to create each predictive map, the modelling parameters, the specific ore-forming process being tested, and statistical results allows for comparisons between predictive maps, which helps with deciding the best combination of proxies to include in the final mineral potential model. This information is recorded in an Excel spreadsheet called a spatial data table. This record is also important if the model is revisited in the future and should contain enough information to make the entire process repeatable (Ford et al., 2019).

In this study, between 49 and 81 predictive maps for each mineral system were produced and tested for spatial correlations with the training data. We inferred a strong spatial correlation from C and StudC values of >2.5 , a moderate correlation from C and StudC values between 1 and 2.5, and weak correlations from C and StudC values < 1 . A summary of key results is provided below for the source, transport, trap, and deposition components of each mineral system. Spatial correlation results are in Appendix A; accompanying spatial files (training points, predictive maps, and posterior probability grids) are in Appendix B ([BCGS_P2024-02.zip](#)).

4.1. Porphyry spatial correlations

4.1.1. Porphyry source

Porphyry mineral systems are typically temporally and spatially associated with highly fractionated intermediate to felsic intrusions, which commonly have porphyritic textures. Felsic to intermediate intrusions and those with porphyritic textures were selected from the bedrock geology map and found to have weak correlations. These rock types were also buffered at 50 m intervals to identify the optimal sphere of influence around the intrusions for known mineralization. The highest correlations were at 2050 m for felsic to intermediate intrusions and 150 m for porphyritic intrusions. All intrusive rocks buffered to 2150 m also had a strong correlation. Magnetic highs interpreted to represent buried intrusions were selected from the residual total field map and showed a moderate correlation with the training data. Together, the magnetic highs and felsic to intermediate intrusions have a weak correlation with the training data. A much stronger correlation was identified when the combined rock types were buffered to 1250 m. Volcanic units queried from the bedrock geology map have a strong spatial correlation at a buffer distance of 2350 m. A combined map of intrusions and volcanic rocks also gave a strong correlation.

Most porphyry deposits in British Columbia were generated in the Triassic and Jurassic, and strong correlation was obtained for rocks formed between ca. 237 Ma and 170 Ma in the study area. Stikine and Quesnel terranes were tested separately; Stikine terrane received a strong correlation whereas Quesnel terrane received no valid statistics. However,

the two terranes combined received a stronger correlation than when independently tested. Given their importance in the region (e.g., Nelson and van Straaten, 2020) the Stuhini Group (Upper Triassic) and Hazelton Group (uppermost Triassic to Middle Jurassic) were also selected and tested individually. Both received moderate correlations but captured few training points. However, with buffer distances of 750 m for the Stuhini Group and 2500 m for the Hazelton Group, stronger spatial correlations were obtained.

4.1.2. Porphyry transport

Faults have long-been recognized as paths for fluid flow. We therefore tested various subsets of fault data including fault length (classified into major, moderate, and minor) and orientation. All faults with an 850 m buffer distance and minor faults with a 450 m buffer correlate best with the training data. Strong correlations were also observed for faults with north, east, and northeast trends.

Intrusive contacts are important paths for fluid flow in porphyry mineral systems. We turned intrusive contacts into polylines that were buffered to test for an association with the training data. The felsic to intermediate intrusion contacts have a high correlation within a 2000 m buffer distance. The combination of intrusive contacts with magnetic high contacts also has a strong correlation with a buffer distance of 1000 m. Porphyritic rock contacts received a strong correlation but captured few training points. The unconformity between the Stuhini and Hazelton groups, also of regional economic significance (e.g., Nelson and Kyba, 2014; Nelson and van Straaten, 2020) was converted to polylines and tested for spatial correlation. The unconformity received a strong correlation, but only captured five training points.

4.1.3. Porphyry trap

Fault intersections, bends, jogs, and splays represent sites that could serve as traps for mineralization. These features were derived from the fault dataset and buffered to test for correlations with the training data. Fault intersections with a buffer distance of 800 m and fault oversteps with a buffer distance of 1550 m both have strong correlations. Fault density may also help highlight potential structural traps. Density maps were created for faults, fault intersections, bends, jogs, and splays using the point and line density tools in Spatial Analyst. The density grids were classified into ten classes and tested for spatial correlation with the training data. High fault density, fault intersection density, and fault bend density all received strong correlations.

4.1.4. Porphyry deposition

Strong correlations for porphyry mineral occurrences and the training data were recorded within a buffer of 7800 m. Commonly found at shallow levels of porphyry systems, high sulphidation epithermal mineral occurrences correlated with training data within 8600 m. Point density grids of the porphyry and high sulphidation epithermal occurrences had strong

correlations. A density map of all metallic mineral occurrences extracted from MINFILE also has a strong correlation with the training data.

Anomalous stream catchment maps for each element (Cu, Pb, Zn, Mo, Ni, Co, Cr, S, Au, Ag, PGE) had only weak to moderate correlations with the training data. Using the average concentration of all the stream-sediment samples collected from a single catchment, copper has a strong correlation and gold, lead, and sulphur all have moderate correlations.

Lithogeochemistry samples anomalous in elements (Cu, Pb, Zn, Mo, Ni, Co, Cr, S, Au, Ag, PGE) were buffered to 2000 m and tested for spatial correlation with the training data (i.e., for contrast and studentized contrast value results, see Appendix A, [BCGS_P2024-02.zip](#)). All the elements tested have weak correlations except for zinc, which has a moderate correlation but with a low number of training points captured. Six training points are in no data areas.

4.2. Volcanogenic massive sulphide spatial correlations

4.2.1. Volcanogenic massive sulphide source

Volcanic and volcanoclastic rocks (including metamorphosed equivalents) were tested as potential source rocks for the volcanogenic massive sulphide mineral system. A buffer of 700 m had the best spatial correlation. Mafic volcanic rocks tested separately received a strong spatial correlation but captured fewer training points. Felsic and mafic volcanic rocks both had moderate correlations but also captured a few training points. Fine-grained siliciclastic rocks, which can be important hosts, had a moderate correlation but extended across a large part of the study area.

4.2.2. Volcanogenic massive sulphide transport

The fault maps tested were the same as those used in the porphyry model. The best correlations were for all faults buffered to 3100 m, minor faults also buffered to 3100 m, north-trending faults buffered to 3050 m, and northwest-trending faults with a 4350 m buffer.

4.2.3. Volcanogenic massive sulphide trap

Fault point datasets were tested as possible traps. The best correlations were for fault intersections (strong correlation at a 1650 m buffer) fault splays (strong correlation at a 3250 m buffer), and fault bends (moderate correlation at a 3450 m buffer). High fault intersection density, high fault bend density, and high fault splay density all have strong correlations with the training data. Gravity maps were classified into ten classes using the quantile method. The best correlations were for the Bouguer gravity map, with a strong correlation, and the free air anomaly map with a moderate correlation.

4.2.4. Volcanogenic massive sulphide deposition

A metallic mineral occurrence density grid was calculated and grouped into ten classes. The moderate to high classes have a strong spatial correlation with the training data and a strong correlation with all classes buffered to 5500 m. Stream

catchment and lithogeochemistry anomaly maps for elements relevant to the mineral system (Cu, Pb, Zn, Au, Ag) were tested for spatial correlation with the training data. The copper stream catchment map, calculated using the average for each catchment, showed a strong correlation. A combined map of copper and gold has a slightly weaker correlation. The gold anomaly map was the only lithogeochemistry map to show a strong correlation. To identify magnetite-destructive alteration that may be associated with volcanogenic massive sulphide mineralization, mapped faults in zones of low magnetic response were selected and buffered. The resulting map has a strong spatial correlation with the training data at a 2650 m buffer.

4.3. Magmatic mafic to ultramafic sulphide spatial correlations

4.3.1. Magmatic mafic to ultramafic sulphide source

A selection of all mafic and ultramafic units gave a strong correlation when buffered to 300 m, as did ultramafic units separately. Selecting only the intrusive rocks improved the spatial correlation significantly and resulted in a very strong correlation, both with no buffer and with a 300 m buffer. Gravity maps were also tested to identify dense rocks that may represent buried or unmapped intrusions. Very similar, strong correlations were observed for gravity highs selected from the isostatic residual, free air anomaly, and first vertical derivative maps. All magnetic maps were tested by classifying the data into ten classes using the quantile method. The best correlations were for magnetic highs from the residual total field and first vertical derivative maps, both receiving high correlation results. The magnetic highs likely correspond to mafic-intermediate (magnetite-bearing) intrusions and volcanic rocks.

4.3.2. Magmatic mafic to ultramafic sulphide transport

The tested fault maps were the same as those used in the porphyry and volcanogenic massive sulphide systems. The best correlations are distance from north-trending faults (4200 m buffer), minor faults (2700 m buffer), northwest-trending faults (4200 m buffer), all faults (2250 m), and distance to medium length faults (2900 m buffer).

4.3.3. Magmatic mafic to ultramafic sulphide trap

Fault point datasets were tested as possible traps. The best correlations were for distance to fault bends (2300 m buffer) and fault splays (5550 m buffer) both receiving strong correlations. Corresponding density maps of these features had weaker correlations. A density map of all faults was created in ArcGIS and has a strong correlation with the training data.

4.3.4. Magmatic mafic to ultramafic sulphide deposition

Stream catchment and lithogeochemistry anomaly maps for Cu, Co, Cr, Zn, Ni, S, PGE, Au, and Ag were tested for spatial correlation with the training data. The copper and cobalt stream catchment maps have strong correlations. A combination of these maps was also tested but had a weaker correlation

than the individual maps. The strongest correlations for the litho-geochemistry data are for cobalt, zinc, and nickel, which received moderate correlations.

5. From predictive maps to mineral potential maps

Mineral potential maps are developed using a selection of the predictive maps created in the spatial analysis process. When separate predictive maps are combined into a final mineral potential map, the weights are calculated independently and then combined. Numerous predictive map combinations may be tested before the final set of maps is chosen. Before selecting which predictive maps to integrate, several items need to be considered. First, each component of the mineral system model (source, transport, and trap) must be represented by at least one predictive map. Second, the selected maps should have moderate to strong statistical correlations with the training data. Third, because informing land-use planning is a key goal of the present work, in cases where predictive maps had similar contrast values, predictive maps that highlighted large areas of mineral potential containing many training points were favoured over predictive maps that restricted areas to few training points. Fourth, the predictive maps must be geologically reasonable with respect to the mineral system being modelled. Finally, combining predictive maps assumes what is referred to as 'conditional independence' in which no predictive map is influenced by another. However, because ore-forming geological processes are commonly interconnected, strict independence is rarely realized and the violation of conditional independence needs to be minimized. Reducing the total number of predictive maps in a final mineral potential model and combining similar predictive map patterns using Boolean operators (e.g., AND, OR; e.g., combining Zn and Pb geochemistry patterns) will reduce the overall violation of the conditional independence assumption (Bonham-Carter, 1994).

The resulting mineral potential maps combine selected predictive maps for the porphyry mineral system (Table 5, Fig. 7), volcanogenic massive sulphide system (Table 6, Fig. 8), and magmatic mafic-ultramafic system (Table 7, Fig. 9). The outputs are posterior probability grids that map the geological potential for mineralization for each grid cell in the form of posterior probability values that range from 0 to 1 (Figs. 10-12). To combine all three mineral systems into a single map of prospectivity over the study area, the posterior probability values were converted into five equal percentile ranking divisions. The maximum percentile ranking for each of the three mineral system maps in each cell in the study area was used as the percentile ranking in the combined mineral potential map (Fig. 13).

6. Validation of mineral potential maps

Validation of the base-case models involved creating success- and prediction-rate curves using ArcSDM's area-frequency tool. In these graphs, either the cumulative captured training point data (success rate) or validation data (prediction rate) are plotted against the cumulative area from highest to

lowest prospectivity. The validation data represent a subset of mineral occurrences that were not used as training points (Fig. 14). For the porphyry and VMS models, validation data consisted of all mineral occurrences excluding training points that were categorized as developed prospects or prospects from MINFILE. We used 112 validation points for the porphyry model and 73 for the VMS model. Due to a lack of developed prospects and prospects with a mafic-ultramafic association, we included showings in the validation dataset, which resulted in 108 points. In general, the greater the area under the curve (reported as an AUC value), and the steeper the gradient of the curve, the better the model is at capturing the training points or validation data within the smallest area (e.g., Chung and Fabbri, 2003; Nykänen et al., 2008). A higher AUC value indicates better efficiency classification of the model, with a perfect classifier having an AUC of 1.0 and a random classifier having an AUC of 0.5. Whereas prediction-rate curves are increasingly being used as a standard validation tool for mineral potential models, a consistent set of standards for evaluating model performance across various studies has yet to be established (Ford et al., 2015, Lawley et al. 2021, 2022). Generally, models that have $AUC > 0.8$ are considered good and > 0.9 as excellent. This method is a test for how effective the model is at reducing the search space for the mineral system considered.

To ensure the validation data were truly independent from the modelling process, base-case models excluded the use of predictive maps made from the validation data (i.e. density of known deposits was excluded). These base-case models were used for validation purposes. However, because some of the predictive maps made from mineral occurrence data had strong correlations with the training data and were relevant to the mineral system, final iterations of the models, referred to as conclusive models, included these maps.

The success-rate curve for the base case mafic-ultramafic sulphide model has the highest AUC value of 0.992, and a slightly lower predictive-rate AUC value of 0.928 (Fig. 14). The base case porphyry model has a success-rate AUC value of 0.974 and the lowest predictive rate of all models with an AUC value of 0.876 (Fig. 14). The VMS base case model has a success AUC value of 0.956 and a relatively similar predictive AUC value of 0.953. Moreover, the base case volcanogenic massive sulphide model captures ~80% of the validation data in 5.82% of the study area. The mafic-ultramafic sulphide base case model captures ~80% of the validation data in 11.85% of study area and the base case porphyry model captures ~80% of the validation data in 23.22% of the study area (Fig. 14).

To further validate the models, the frequency of validation data is tested against ten equal percentile divisions based on posterior probability values of the respective mineral system (Table 8). The greater the number of validation data captured in the higher percentile divisions, the better the model is at predicting sites of mineralization for that mineral system, regardless of the size of the prospective areas. In general, the base-case models for the porphyry and mafic-ultramafic mineral systems capture 76% and 84% respectively of the

Wearmouth, Czertowicz, Peters, Orovan

Table 5. Statistical spatial analysis results for predictive maps used in the porphyry model.

Mineral system component	Spatial variable	Variable ID	# TP	C	StudC
Source	Distance to volcanic rocks	2350 m	11	3.0	2.9
	Distance to intermediate and felsic intrusive rocks and high total residual total field mag areas (inferred intrusions)	Class 9-10 (>160 nT/m), felsic intrusive, 1000 m	11	4.0	3.8
Transport	Distance to all faults	850 m	10	3.0	3.8
	Distance to intermediate and felsic intrusive rocks and high total residual total field mag contacts	Class 9-10 (>160 nT/m), felsic intrusive, 1250 m	12	3.1	2.9
Trap	Fault intersection density	Class 4-10 (moderate to high density)	12	2.7	2.6
Deposition	Ag stream anomalies	Ag > 0.33 ppm	11	2.0	1.9
	Au stream anomalies	Au > 0.01 ppm	12	1.9	1.8
	Cu stream anomalies	Cu > 106.05 ppm	10	1.9	2.5
	Density of porphyry + HS epithermal occurrences + rock chips anomalous in Cu or Zn	Class 4-10 (high density)	11	3.56	3.38

Table 6. Statistical spatial analysis results for predictive maps used in the volcanogenic massive sulphide model.

Mineral system component	Spatial variable	Variable ID	# TP	C	StudC
Source	Distance to prospective stratigraphy	300 m	11	3.4	3.3
	Distance to volcanic and volcanoclastic rocks (and metamorphosed equivalents)	300 m	9	3.2	4.1
Transport	Distance to minor faults	3100 m	10	3.0	2.8
Trap	Fault intersection density	Class 5-10 (moderate to high density)	9	2.2	2.8
Deposition	Stream sediment Cu + Au anomaly (mean, reclassified)	(Cu = 106.05, Au = 0.01) ppm	10	2.5	2.4
	Stream sediment Zn + Pb + Ag anomaly (mean, reclassified)	(Zn = 183.55, Pb = 18.87, Ag = 0.33) ppm	6	0.9	1.4
	Density of VMS occs - update + Zn, Pb, Ag rock chip anomalies	Class 6-10 (high density)	10	4.6	4.3

Table 7. Statistical spatial analysis results for predictive maps used in the magmatic mafic-ultramafic model.

Mineral system component	Spatial variable	Variable ID	# TP	C	StudC
Source	Distance to ultramafic or mafic intrusive rocks	300 m	6	5.0	6.1
Transport	Distance to minor faults	2700 m	7	2.8	2.6
Trap	Magnetics 1st vertical derivative	Class 8 – 10 (>0.0085 nT/m)	7	3.0	2.8
	Fault density	Class 7-10 (high density)	8	2.4	2.2
Deposition	Gravity isostatic residual	Class 7 – 10 (>9.50 mGal)	7	2.4	2.2
	Stream sediment Co anomaly	33.05 ppm	7	2.4	2.2
	Density of UM/M intrusive mineral occurrences + rock chips anomalous in Ni or Co or Zn	Class 5-10 (high density)	7	3.9	3.6

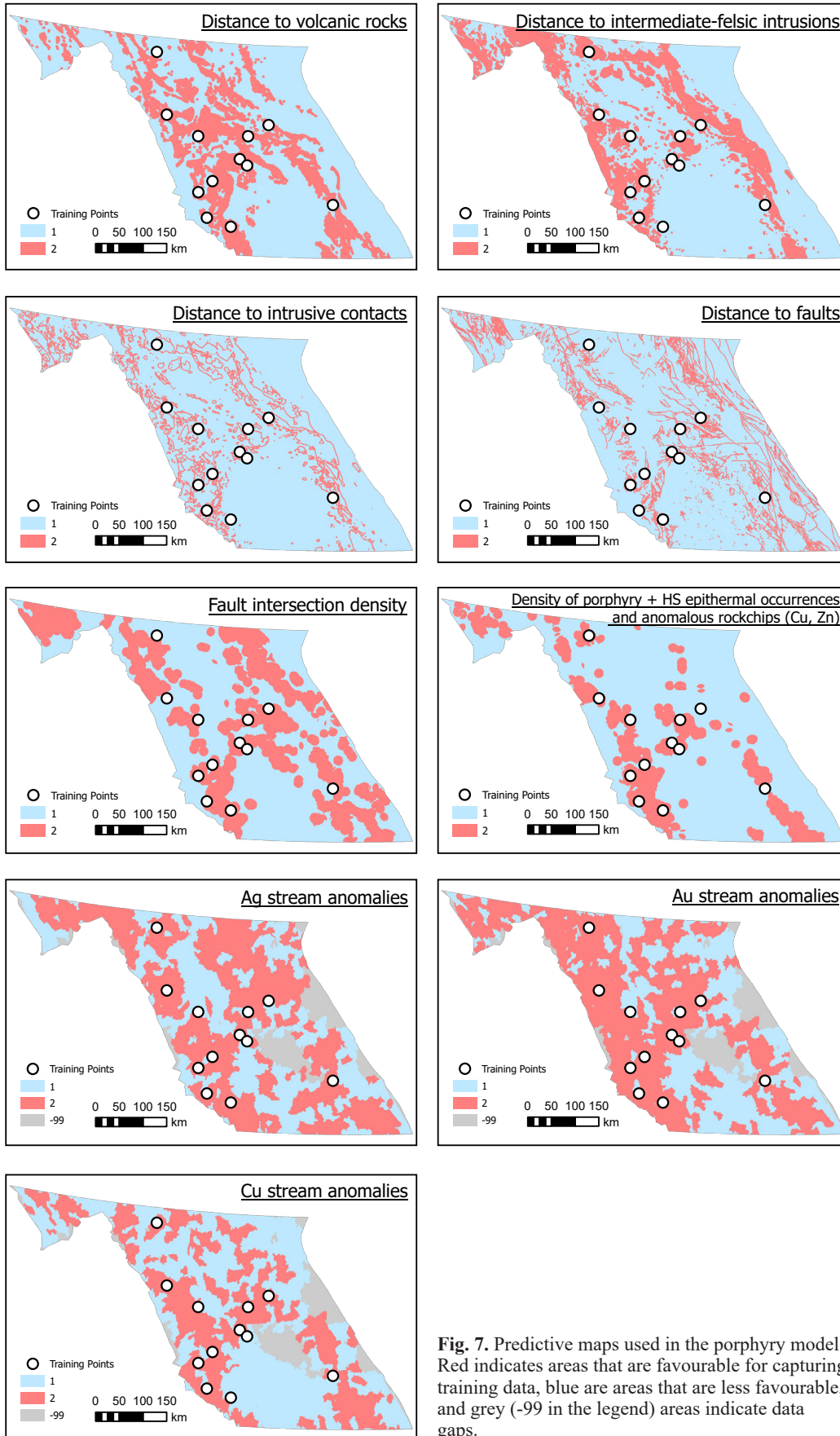


Fig. 7. Predictive maps used in the porphyry model. Red indicates areas that are favourable for capturing training data, blue are areas that are less favourable, and grey (-99 in the legend) areas indicate data gaps.

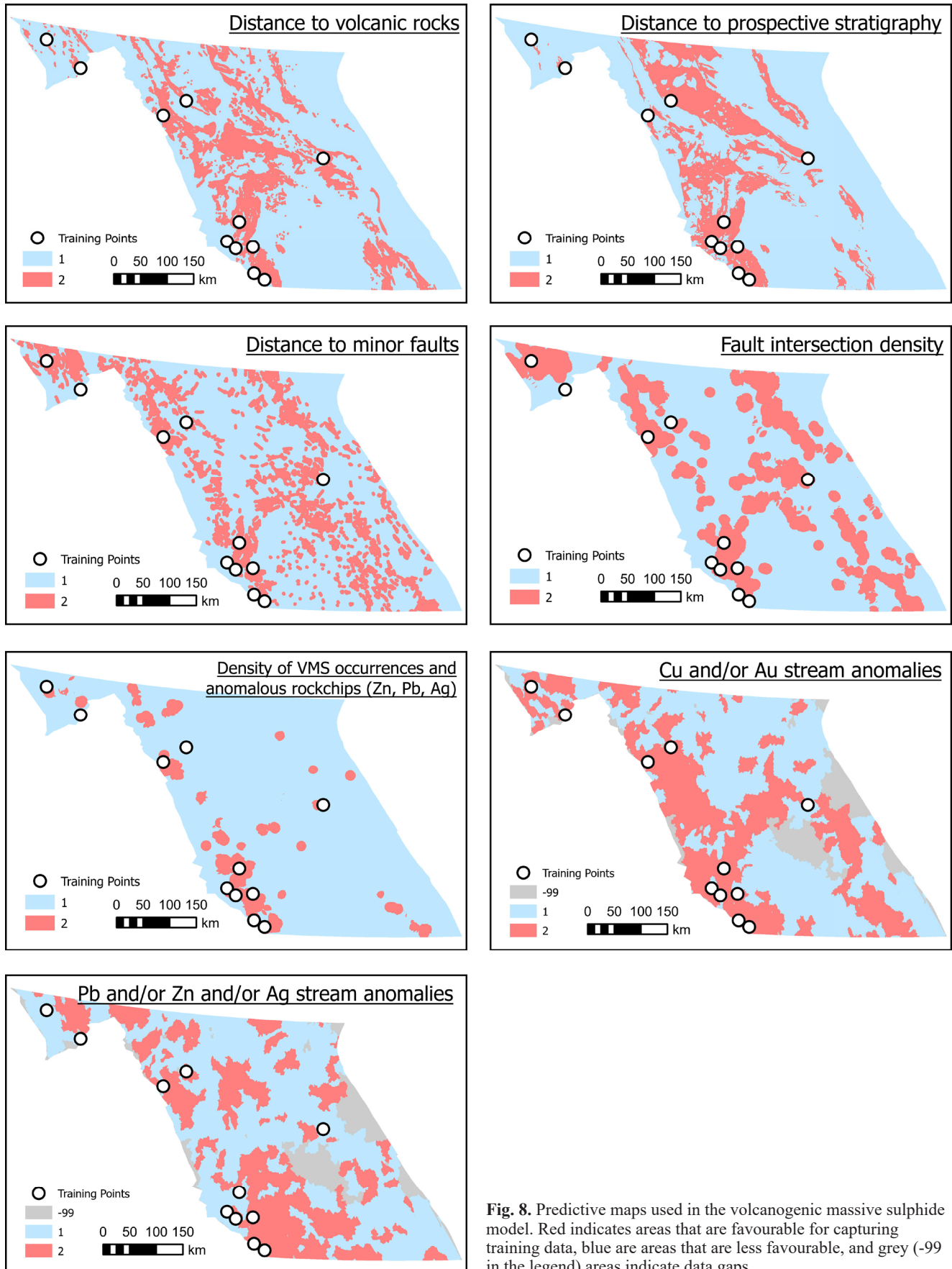


Fig. 8. Predictive maps used in the volcanogenic massive sulphide model. Red indicates areas that are favourable for capturing training data, blue are areas that are less favourable, and grey (-99 in the legend) areas indicate data gaps.

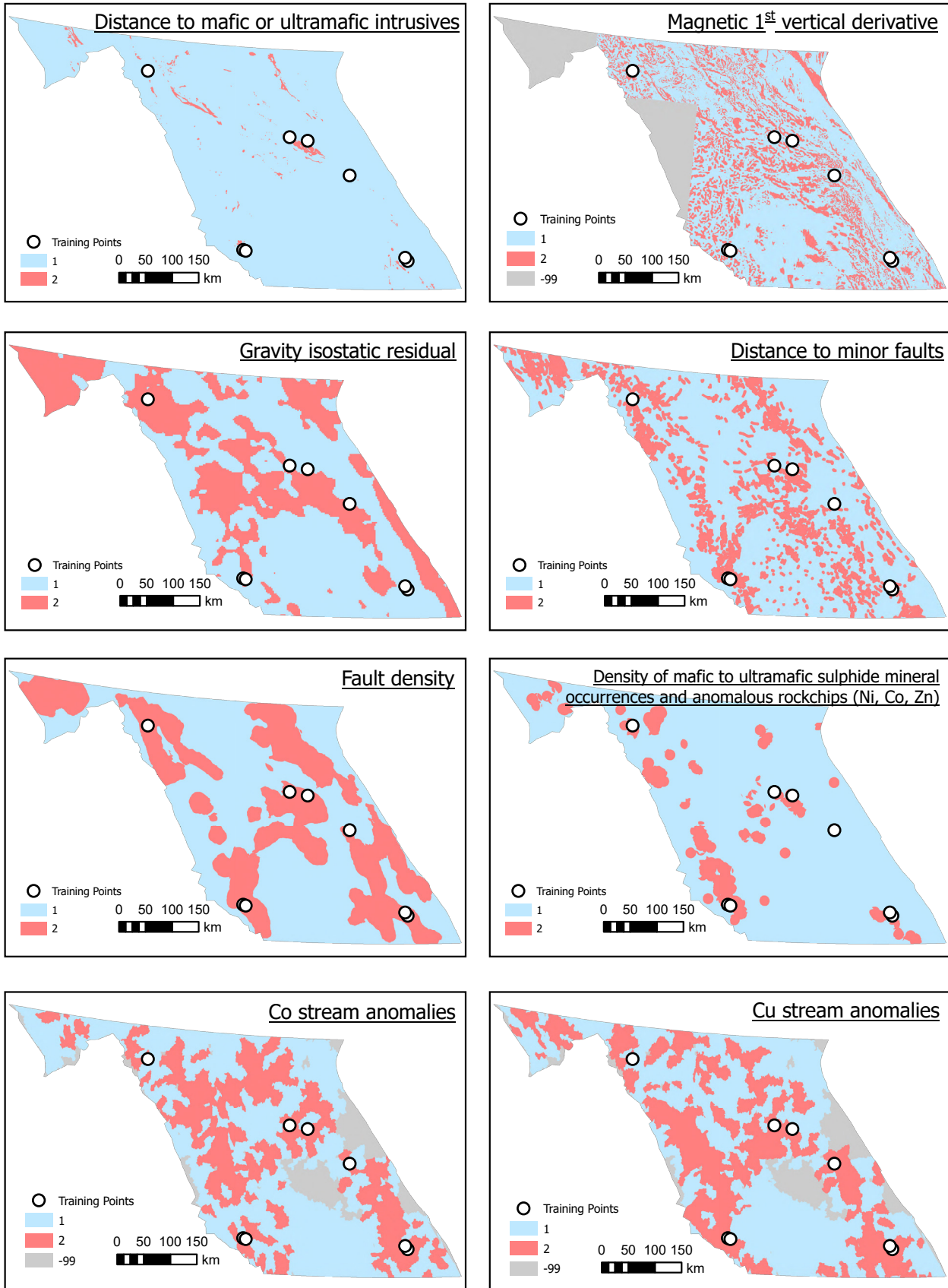


Fig. 9. Predictive maps used in the magmatic mafic to ultramafic model. Red (1 in the legend) indicates areas that are favourable at capturing training data, blue (2 in the legend) is less favourable, and grey (-99 in the legend) areas indicate data gaps.

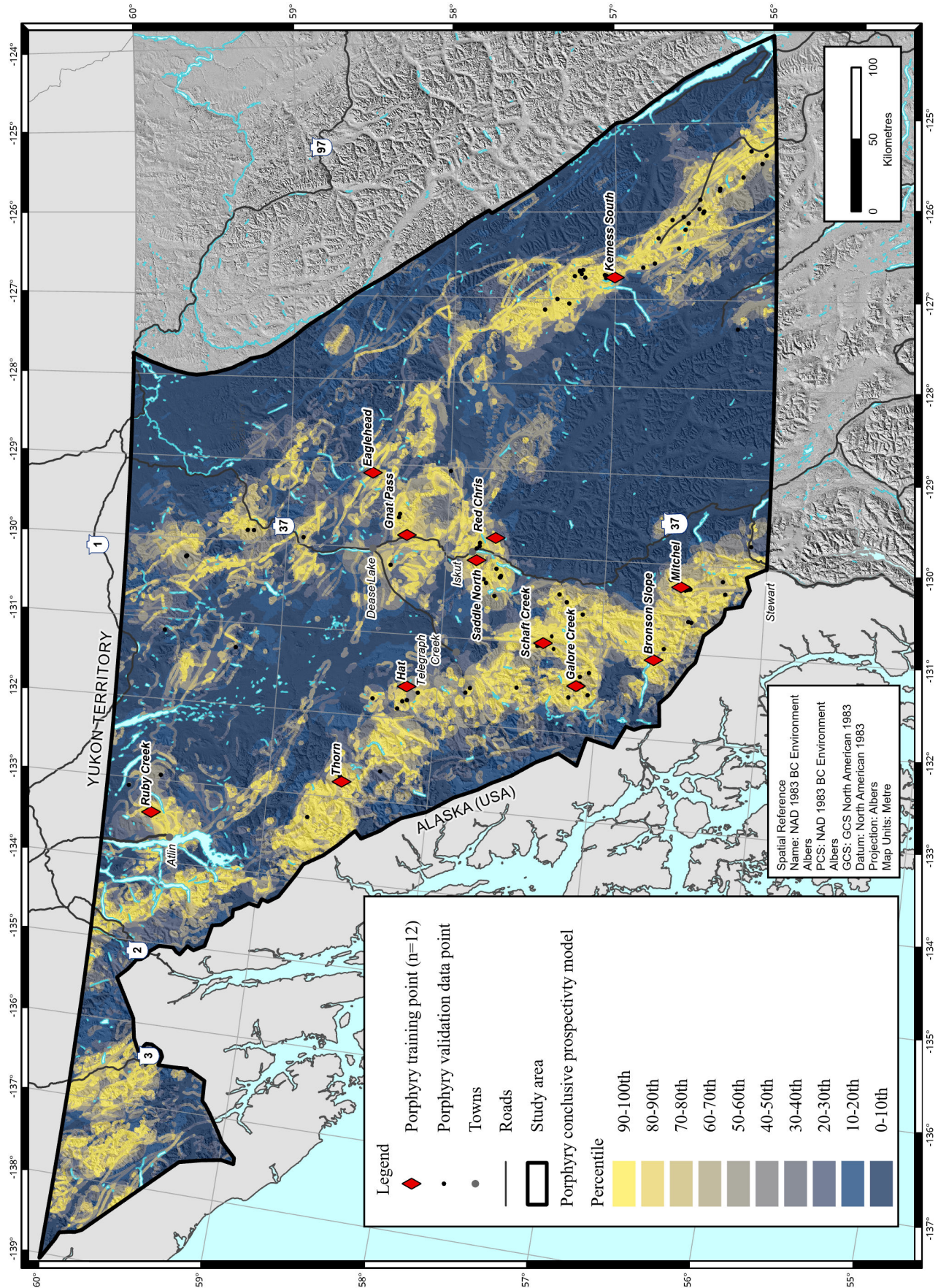


Fig. 10. Porphyry mineral potential map displaying the calculated posterior probability grid values for mineralization for each grid cell depending on the combination of weighted predictive map variables for the conclusive model. Posterior probability values are ranked into ten equal percentile divisions with the highest values in yellow.

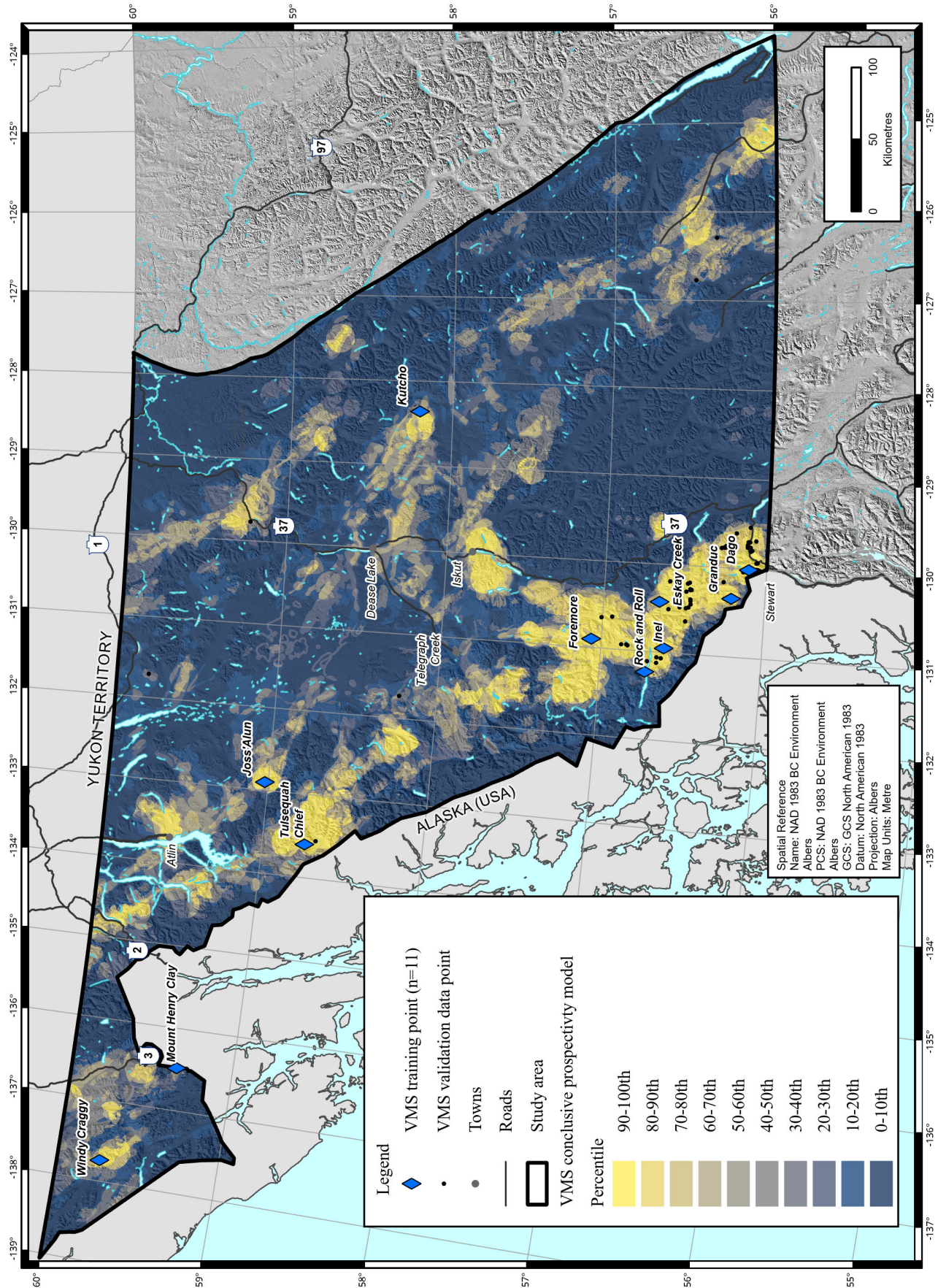


Fig. 11. Volcanogenic massive sulphide mineral potential map displaying the calculated posterior probability grid values for the conclusive model. Posterior probability values are ranked into ten equal percentile divisions with the highest values in yellow.

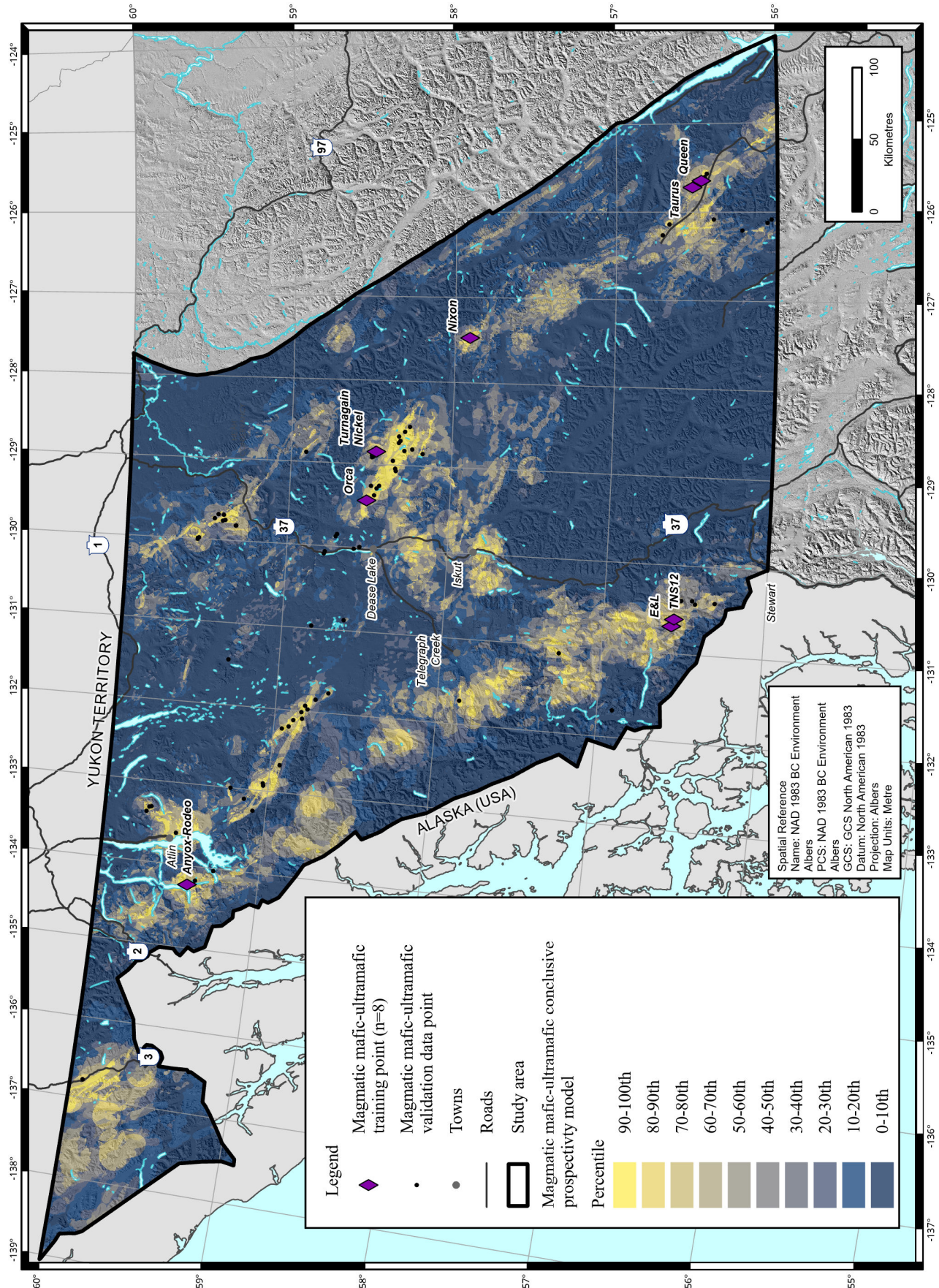


Fig. 12. Magmatic mafic to ultramafic sulphide mineral potential map displaying the calculated posterior probability grid values for the conclusive model. Posterior probability values are ranked into ten equal percentile divisions with the highest values in yellow.

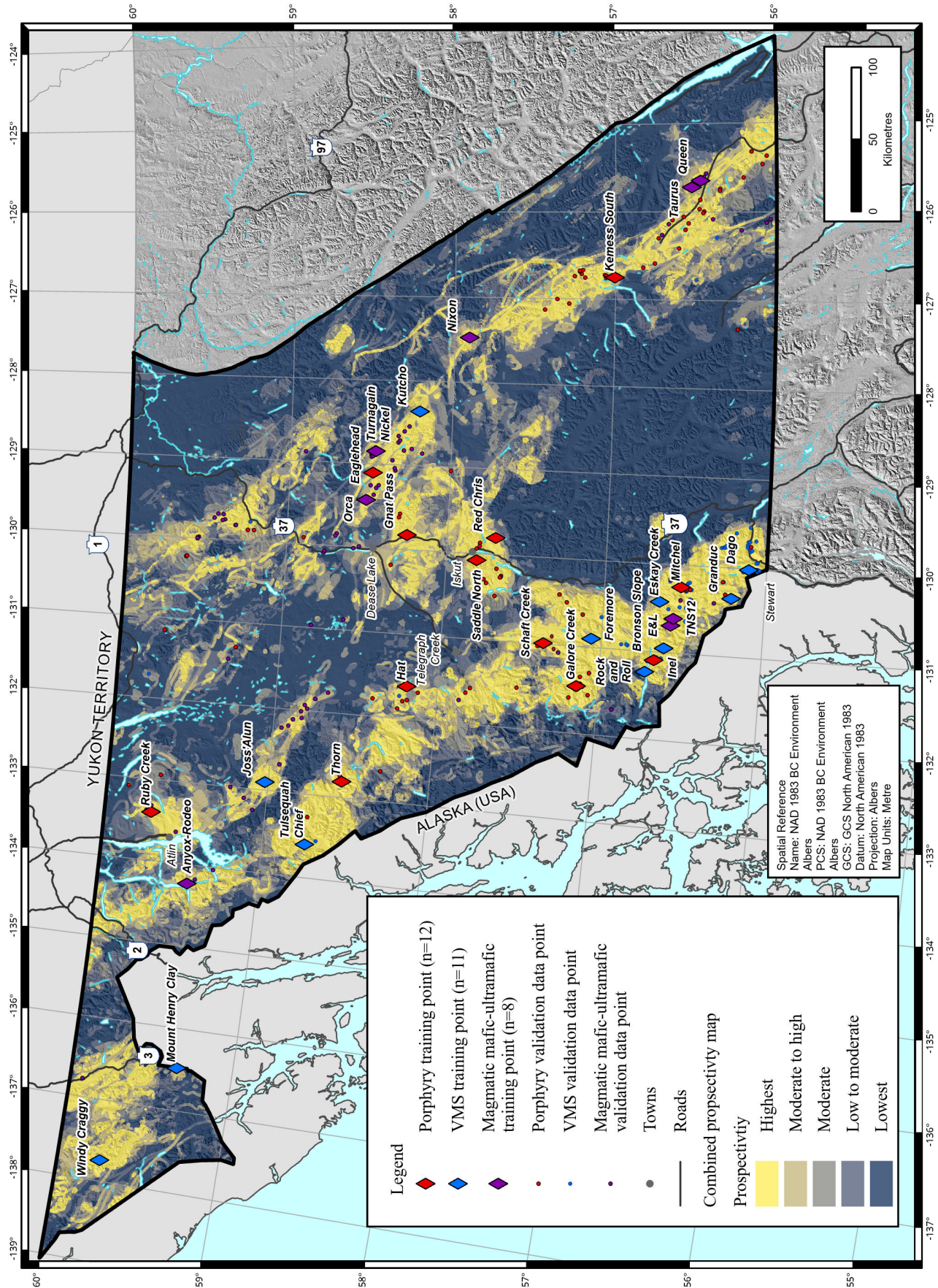


Fig. 13. Combined mineral potential map using the conclusive models for porphyry, volcanogenic massive sulphide and magmatic mafic-ultramafic deposits displaying the maximum combined percentile ranking of all three mineral systems. Maps were combined by converting the posterior probability values for each map into five equal percentile ranking divisions. The maximum percentile ranking for each of the three mineral system maps at each cell within the study area was used as the percentile ranking.

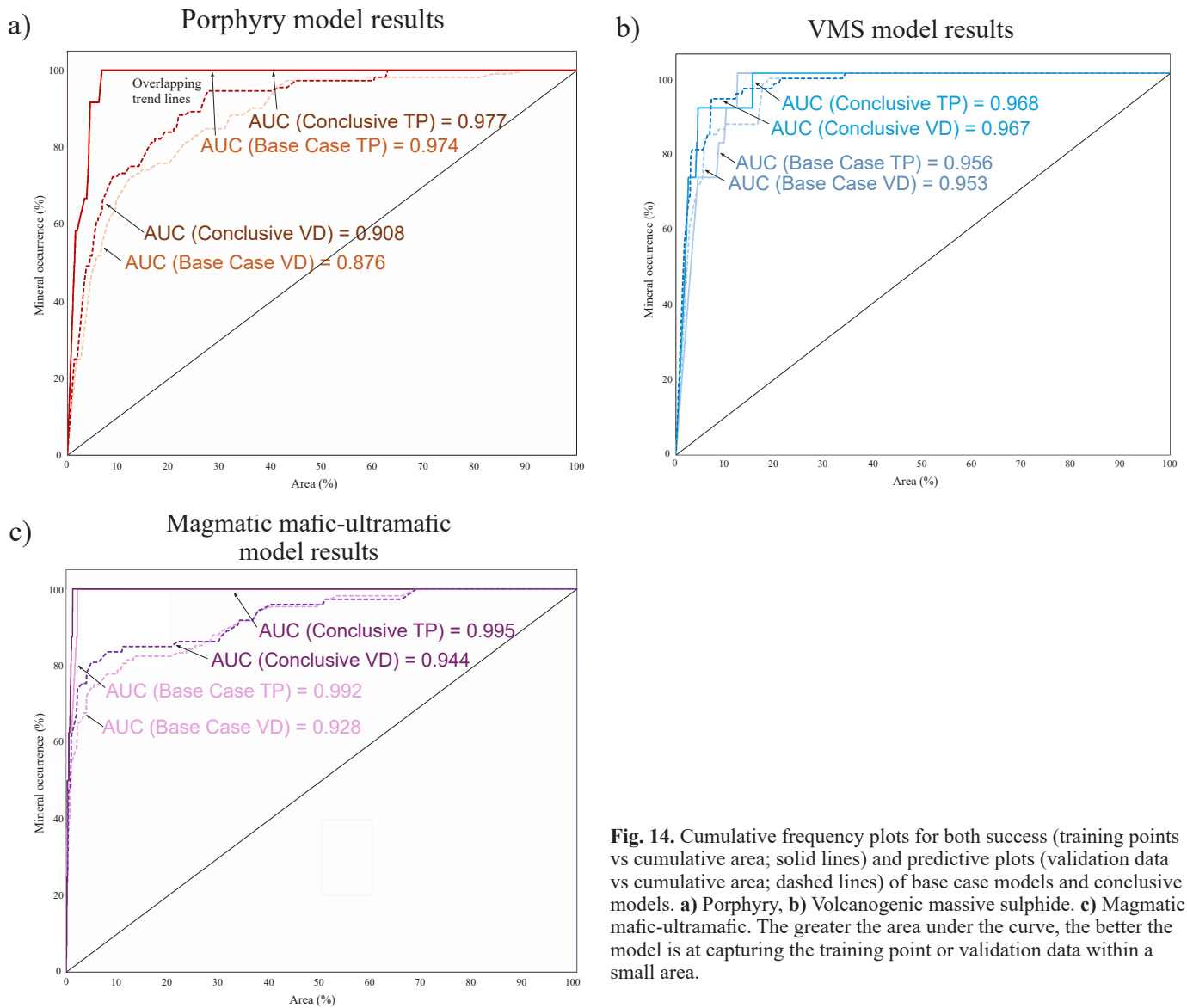


Fig. 14. Cumulative frequency plots for both success (training points vs cumulative area; solid lines) and predictive plots (validation data vs cumulative area; dashed lines) of base case models and conclusive models. **a)** Porphyry, **b)** Volcanogenic massive sulphide. **c)** Magmatic mafic-ultramafic. The greater the area under the curve, the better the model is at capturing the training point or validation data within a small area.

Table 8. Distribution of validation data for each mineral system within each tenth percentile division.

Hierarchy	Percentile	Porphyry		VMS		Magmatic mafic-ultramafic	
		Base	Conclusive	Base	Conclusive	Base	Conclusive
Highest	100-90	55.4%	72.3%	85.3%	95.9%	54.8%	73.2%
	90-80	17.9%	2.7%	1.3%	0.0%	19.2%	8.5%
High to moderate	80-70	2.7%	8.9%	0.0%	0.0%	6.8%	4.2%
	70-60	0.0%	4.5%	12.0%	0.0%	2.7%	1.4%
Moderate	60-50	8.9%	6.3%	0.0%	1.4%	1.4%	0.0%
	50-40	3.6%	0.0%	0.0%	1.4%	1.4%	5.6%
Moderate to low	40-30	8.9%	0.0%	1.3%	0.0%	0.0%	0.0%
	30-20	0.0%	2.7%	0.0%	1.4%	8.2%	0.0%
Lowest	20-10	0.9%	2.7%	0.0%	0.0%	2.7%	2.8%
	10-0	1.8%	0.0%	0.0%	0.0%	2.7%	4.2%

n = 112

n = 73

n = 108

validation data in the top 70th percentile and the volcanogenic mineral system captures 87% of the validation data in the top 70th percentile. These three models capture similar amounts of validation data (between 90 and 99% of the validation data) within the 50-40th percentile. As expected, including the use of the validation data in the form of predictive maps for the conclusive models increased the number of validation data points captured in the highest percentile divisions. The conclusive porphyry and magmatic mafic-ultramafic model captured 72.3% and 73.2% of the validation data in the top 90th percentile division, while the VMS conclusive model captured 95.9% of the validation data in the 90th percentile.

7. Discussion

Although the techniques in this mineral potential modeling assessment are referred to as being data driven, an element of expert biases is present throughout the workflow, as is the case for many mineral potential models. Additionally, different modelling objectives (e.g., drill hole targeting vs land use planning) can affect the decision-making process throughout the workflow resulting in different outcomes. However, with the workflow and predictive maps documenting the modelling process, and when made freely available, different valid models can be produced using different combinations of predicative maps to fit the needs of additional users with different objectives in mind.

Commonly, the goal of published mineral potential models is to reduce the exploration search space to a minimum and therefore increase the likelihood of discovering a mineral deposit (e.g., Harris and Sanborn-Barrie, 2006; Ford et al. 2015; Lawley et al., 2021, 2022; Nykanen et al., 2023). One objective of this modelling project was to quantitatively produce an easily understandable and consumable ranking of mineral potential. Although search area reduction was still an important consideration, and achieved at a regional scale, the objective of the modelling was to also identify areas of moderate and low mineral potential. Still, the conclusive models presented here can delineate areas of high mineral potential by reclassifying the conclusive mineral potential models, which may then identify areas of focus for detailed exploration. Here, we compare the results of the three mineral systems relative to one another from within the same study area.

The base-case VMS model was the most efficient at capturing the validation data points in the least amount of area (AUC = 0.953). Interestingly this base-case VMS model had a similar AUC value for the training data (AUC = 0.956), which may suggest that the training points and predictive maps used in the VMS model accurately represent VMS mineral occurrences in the region. The base-case mafic-ultramafic sulfide model is extremely efficient in predicting the training data (AUC of 0.992), but slightly less efficient at predicting the validation data (AUC of 0.928). This is similar to the base-case porphyry model that had a success rate AUC value of 0.974 and a predictive AUC value of 0.876. This amount of variation may likely be due to sub-types of mineral systems within the validation data.

Sub-types of mineral systems have greater variability regarding the mineral system components (source, transport, and trap) that make up the mineral system. If the variability is great enough in the validation data compared the training data, it can be problematic to predict the location of the sub-type mineral systems because the models are trained to predict the location of mineral systems akin to the training data. This was a particular concern at the onset of the modelling project, yet all models performed well with AUC values >0.876. This may suggest the predictive maps used in the models accurately capture potential sub-type mineral systems within the study area. Additionally, the base-case models for both the porphyry and magmatic mafic-ultramafic mineral systems have similar AUC scores of 0.876 and 0.928 suggesting that both models have a similar ability to predict the location of known mineralization in the study area. However, the predictive curves suggest the study area is most prospective for porphyries by area.

8. Limitations and uncertainties

The mineral potential modelling comes with several caveats. First, the final maps represent the relative ranking of cells rather than an absolute measure of the probability of finding a deposit (Bonham-Carter et al., 1990; Bonham-Carter, 1994; Ford et al., 2019). This is because conditional independence is violated in all three models and the posterior probabilities are likely overestimated. Second, mineral potential evaluations have uncertainties related to data availability, data quality, the level of correlation between mineral occurrences and the input data, the estimation method, and the deposit model that are partially cumulative and difficult to adequately address (e.g., Harmel et al., 2006). Because of these uncertainties, the potential assessments cannot be used to indicate the size or economics of a potential mineral deposit and cannot be used to make valuations on any resource. Third, any modelling is limited by the data available at any given time and thus the results represent a time-specific evaluation (Ford et al., 2019). For example, areas with a very low mineral potential ranking may merely reflect a paucity of data. In addition, the MINFILE database may not be entirely comprehensive because older records continue to be revised and some critical minerals are likely underreported because they were not historically considered by the exploration community or because past analytical technology may have been inadequate to test for some elements. Future iterations may consider additional datasets or advancements in mineral system research, which may affect the results. Fourth, the prospectivity thresholds rankings purposed here, ‘lowest, low to moderate, moderate, moderate to high, and highest’ are based on five percentile divisions of the posterior probabilities for the mineral potential models. Importantly, the use of percentiles to arbitrarily define prospectivity thresholds is one of many methods (e.g., natural breaks, equal area binning, and custom binning) that can be used to define thresholds of prospectivity. Therefore, using another method to define prospectivity thresholds may not lead to the same conclusions derived in this study. Finally,

the current maps only consider three mineral systems, and the relative prospectivity portrayed on the combined mineral potential map (Fig. 13) may change markedly as additional mineral systems are considered.

9. Conclusions

The methods presented herein demonstrate how mineral systems can be modelled across broad areas of British Columbia to produce mineral potential maps that update work done in the 1990s. The approach we use translates the key ore-forming components of porphyry, volcanogenic massive sulphide, and magmatic mafic-ultramafic sulphide mineral systems into mappable proxies that can be tested with spatial statistics using training data and the data-driven weights of evidence technique. Future work could consider other mineral systems (e.g., epithermal deposits) and could employ different modelling techniques such as fuzzy logic or random forests and, in areas with extensive data, advanced AI systems. This new mineral potential modelling will be one of many pieces of information that will help guide land-use decisions. As society places more value on the transition to a low-carbon future, demand for minerals important for energy generation, storage, and transmission will increase. The new modelling will aid in the search for ‘traditional’ primary critical elements such as copper, but also for companion critical elements which, occurring in small amounts, were previously overlooked or considered uneconomic.

Acknowledgements

We thank Nate Corcoran, Yao Cui, Fil Ferri, Kirk Hancock, Mitch Mihalynuk, JoAnne Nelson, Graham Nixon, Luke Ootes, Paul Schiarizza, and Bram van Straaten for providing valuable feedback on the results. Special thanks to Paulina Marczak for GIS support and map production. Thanks to Christopher Lawley for a perceptive review that helped improve this paper.

References cited

- Agterberg, F.P., Bonham-Carter, G.F., and Wright, D.F., 1990. Statistical pattern integration for mineral exploration. In: Gaal, G., and Merriam, D.F., (Eds.) *Computer Applications in Resource Estimation*, Elsevier, pp. 1-21.
<<https://doi.org/10.1016/B978-0-08-037245-7.50006-8>>
- Barnes, S.-J., and Lightfoot, P.C., 2005. Formation of magmatic nickel-sulfide ore deposits and processes affecting their copper and platinum group element contents. In: Hedenquist, J.W., Thompson, J.F.H., Goldfarb, R.J., and Richards, J.P. (Eds.) *Economic Geology 100th Anniversary Volume*, pp. 179-213.
- Barresi, T., Nelson, J.L., and Dostal, J., 2015. Geochemical constraints on magmatic and metallogenic processes: Iskut River Formation, volcanogenic massive sulfide-hosting basalts, NW British Columbia, Canada. *Canadian Journal of Earth Sciences*, 52, 1-20.
<<https://cdnsiencepub.com/doi/10.1139/cjes-2014-0034>>
- Bonham-Carter, G., 1994. *Geographic information systems for geoscientists: Modelling with GIS* Pergamon, 398 p.
- Bonham-Carter, G.F., Agterberg, F.P., and Wright, D.F., 1990. Weights of evidence modelling: a new approach to mapping mineral potential. In: Agterberg F.P., and Bonham-Carter G.F., (Eds.), *Statistical Applications in the Earth Sciences*. Geological Survey of Canada, Paper 89-09, pp. 171-183.
- British Columbia Geological Survey, 2023. *The Golden Triangle of northwestern British Columbia*. British Columbia Ministry of Energy, Mines and Petroleum Resources, British Columbia Geological Survey Information Circular 2023-05, 6p. (brochure)
- Brew, D.A., 1992. Decision points and strategies in quantitative probabilistic assessment of undiscovered mineral resources. *US Geological Survey, Open File 92-308*, 23 p.
<<https://doi.org/10.3133/of92307>>
- Bustard, A.L., Han, T., and Ferbey, T., 2017. *Compiled till geochemical data for British Columbia*. British Columbia Ministry of Energy, Mines and Petroleum Resources, British Columbia Geological Survey GeoFile 2017-09, 7 p.
- Bustard, A.L., Ferbey, T., and Arnold, H., 2019. *Regional- to property-scale till geochemical and mineralogical surveys in British Columbia for base and precious metals*. British Columbia Ministry of Energy and Mines and Petroleum Resources, British Columbia Geological Survey Open File 2019-04, version 2020-01.
- Chung C. F., and Fabbri A. G., 2003. Validation of spatial prediction models for landslide hazard mapping. *Natural Hazards* 30, 451-472.
- Clarke, G., Northcote, B., Corcoran, N.L., Pothorin, C., Heidarian, H., and Hancock, K., 2024. *Exploration and Mining in British Columbia, 2023: A summary*. In: *Provincial overview of exploration and mining in British Columbia, 2023*. British Columbia Ministry of Energy, Mines and Low Carbon Innovation, British Columbia Geological Survey Information Circular 2024-01, pp. 1-53.
- Colpron, M., 2020. *Yukon terranes-A digital atlas of terranes for the northern Cordillera*. Yukon Geological Survey.
<<https://data.geology.gov.yk.ca/Compilation/2#InfoTab>>
- Colpron, M., and Nelson, J.L., 2021. Northern Cordillera: Canada and Alaska. In: Elias, S., and Alderton, D., (Eds.), *Encyclopedia of Geology*, Second Edition. Academic Press, pp. 93-106.
- Cousens, B., and Piercey, S.J., (Eds.), 2008. *Submarine volcanism and mineralization: Modern through ancient*. Geological Association of Canada Short Course Notes Volume 19, 178 p.
- Cui, Y., Miller, D., Schiarizza, P., and Diakow, L.J., 2017. *British Columbia digital geology*. British Columbia Ministry of Energy, Mines and Petroleum Resources, British Columbia Geological Survey, Open File 2017-8, 9p. Data version 2019-12-19.
- Febbo, G.E., Kennedy, L.A., Nelson, J.L., Savell, M.J., Campbell, M.E., Creaser, R.A., Friedman, R.M., van Straaten, B.I., Stein, H.J., 2019. The evolution and structural modification of the supergiant Mitchell Au-Cu porphyry, northwestern British Columbia. *Economic Geology*, 114, 303-324.
- Ford, A., 2020. Practical implementation of random forest-based mineral potential mapping for porphyry Cu-Au mineralization in the Eastern Lachlan Orogen, NSW, Australia. *Natural Resources Research*, 29, 267-283.
<<https://doi.org/10.1007/s11053-019-09598-y>>
- Ford, A., Miller, J.M., and Mol, A.G., 2015. A comparative analysis of weights of evidence, evidential belief functions, and fuzzy logic for mineral potential mapping using incomplete data at the scale of investigation. *Natural Resources Research*, 25, 19-3.
<<https://doi.org/10.1007/s11053-015-9263-2>>
- Ford, A., Peters, K.J., Partington, G.A., Blevin, P.L., Downes,

- P.M., Fitzherbert, J.A., and Greenfield, J.E., 2019. Translating expressions of intrusion-related mineral systems into mappable spatial proxies for mineral potential mapping: Case studies from the Southern New England Orogen, Australia. *Ore Geology Reviews*, 111, article 102943.
<<https://doi.org/10.1016/j.oregeorev.2019.102943>>
- Franklin, J.M., Gibson, H.L., Jonasson, I.R., and Galley, A.G., 2005. Volcanogenic massive sulfide deposits. In: Hedenquist, J.W., Thompson, J.F.H., Goldfarb, R.J., and Richards, J.P., (Eds.), *Economic Geology 100th Anniversary Volume*, pp. 523-560.
- Galley, A.G., Hannington, M.D., and Jonasson, I.R., 2007. Volcanogenic massive sulphide deposits. In: Goodfellow, W.D., (Ed.), *Mineral deposits of Canada*. Geological Association of Canada, Mineral Deposits Division, Special Publication 5, pp. 141-161.
- Groves, D.L., Santosh, M., Müller, D., Zhang, L., Deng, J., Yang, L., and Wang, Q., 2022. Mineral systems: Their advantages in terms of developing holistic genetic models and for target generation in global mineral exploration. *Geosystems and Geoenvironment*, 1, article 100001.
<<https://doi.org/10.1016/j.geogeo.2021.09.001>>
- Grunsky, E.C., 1997. Mineral resource estimation: the Mineral Potential Project: an evaluation of estimator responses for selected mineral deposit types for the province. In: *Geological Fieldwork 1997*, British Columbia Ministry of Employment and Investment, British Columbia Geological Survey, Paper 1997-01, pp. 267-282.
- Han, T., and Rukhlov, A.S., 2020a. Update of the provincial Regional Geochemical Survey (RGS) database at the British Columbia Geological Survey. British Columbia Ministry of Energy, Mines and Petroleum Resources, British Columbia Geological Survey GeoFile 2020-08, 3 p.
- Han, T., and Rukhlov, A.S., 2020b. Update of rock geochemical database at the British Columbia Geological Survey. British Columbia Ministry of Energy, Mines and Petroleum Resources, British Columbia Geological Survey GeoFile 2020-02, 4 p.
- Harmel, R.D., Cooper R.J., Slade R.M., Haney R.L., and Arnold, J.G., 2006. Cumulative uncertainty in measured streamflow and water quality data for small watersheds. *Transactions of the American Society of Agricultural and Biological Engineers*, 49, 689-701.
- Harris, J. R., and Sanborn-Barrie, M., 2006. Mineral potential mapping: Examples from the Red Lake Greenstone Belt, Northwest Ontario. In: J.R. Harris (Ed.) *GIS for the Earth Sciences*, Geological Association of Canada Special Publication 44, pp. 1-21.
- Harris, J.R., Grunsky, E., Behnia, P., and Corrigan, D., 2015. Data and knowledge-driven mineral prospectivity maps for Canada's north. *Ore Geology Reviews*, 71, 788-803.
<<https://doi.org/10.1016/j.oregeorev.2015.01.004>>
- Hickin, A.S., and Plouffe, A., 2017. Sampling and interpreting stream, lake, and glacial sediments for mineral exploration in the Canadian Cordillera, a review. In: Ferbey, T., Plouffe, A., and Hickin, A.S., (Eds.), *Indicator Minerals in Till and Stream Sediments of the Canadian Cordillera*. Geological Association of Canada Special Paper Volume 50, and Mineralogical Association of Canada Topics in Mineral Sciences Volume 47, pp. 27-51.
- Hickin, A.S., Ward, B.C., Plouffe, A., and Nelson, J., 2017. Introduction to the geology, physiography, and glacial history of the Canadian Cordillera in British Columbia and Yukon. In: Ferbey, T., Plouffe, A., and Hickin, A.S., (Eds.), *Indicator Minerals in Till and Stream Sediments of the Canadian Cordillera*. Geological Association of Canada Special Paper Volume 50, and Mineralogical Association of Canada Topics in Mineral Sciences Volume 47, pp. 1-25.
- Hickin, A.S., Orovan, E.A., Brzozowski, M.J., McLaren, K., Shaw, K.L., and Van der Vlugt, J., 2023. *Critical minerals in British Columbia: An atlas of occurrences and producing mines, 2023*. British Columbia Ministry of Energy, Mines and Low Carbon Innovation, British Columbia Geological Survey Open File 2023-02 102p.
- Hickin, A.S., Ootes, L., Orovan, E.A., Brzozowski, M.J., Northcote, B.K., Rukhlov, A.S., and Bain, W.M., 2024. Critical minerals and mineral systems in British Columbia. In: *Geological Fieldwork 2023*, British Columbia Ministry of Energy, Mines and Low Carbon Innovation, British Columbia Geological Survey Paper 2024-01, pp. 13-51.
- Hronsky, J.M.A., and Groves, D.I., 2008. The science of targeting: definition, strategies, targeting and performance measurement. *Australian Journal of Earth Science*, 55, 3-12.
<<https://doi.org/10.1080/08120090701581356>>
- Hunter, R.C., Seibert, C.F.B., Friedman, R., and Wall, C., 2022. Revised stratigraphy and geochronology of the Hazelton Group, host rocks for volcanogenic mineralization in the Kitsault River area, northwest British Columbia. In: *Geological Fieldwork 2021*, British Columbia Ministry of Energy, Mines and Low Carbon Innovation, British Columbia Geological Survey Paper 2022-01, pp. 63-81.
- Kilby, W.E., 1995. Mineral potential project-overview. In: *Geological Fieldwork 1994*, British Columbia Ministry of Energy, Mines and Petroleum Resources, British Columbia Geological Survey, Paper 1995-1, pp. 411-416.
- Kilby, W.E., 1996. Mineral potential assessment projects-An update. In: *Geological Fieldwork 1995*, British Columbia Ministry of Energy, Mines and Petroleum Resources, British Columbia Geological Survey, Paper 1996-1, pp. 301-308.
- Kilby, W.E., 2004. The British Columbia mineral potential project 1992-1997 - methodology and results. Ministry of Energy and Mines, British Columbia Geological Survey, GeoFile 2004-2, 324 p.
- Knox-Robinson, C.M. and Wyborn, L.A.I., 1997. Towards a holistic exploration strategy: using geographic information systems as a tool to enhance exploration. *Australian Journal of Earth Scientists* 44, 453-463.
<<https://doi.org/10.1080/08120099708728326>>
- Kreuzer, O.P., Miller, A.V.M., Peters, K.J., Payne, C., Wildman, C., Partington, G.A., Puccioni, E., McMahon, M.E., and Etheridge, M.A., 2015. Comparing prospectivity modelling results and past exploration data: A case study of porphyry Cu–Au mineral systems in the Macquarie Arc, Lachlan Fold Belt, New South Wales. *Ore Geology Reviews*, 71, 516-544.
<<https://doi.org/10.1016/j.oregeorev.2014.09.001>>
- Lawley, C.J.M., Tschirhart, V., Smith, J.W., Pehrsson, S.J., Schetselaar, E.M., Schaeffer, A.J., Houli, M.G., and Eglinton, B.M., 2021. Prospectivity modelling of Canadian magmatic Ni (±Cu±Co±PGE) sulphide mineral systems. *Ore Geology Reviews*, 132.
<<https://doi.org/10.1016/j.oregeorev.2021.103985>>
- Lawley, C.J.M., McCafferty, A.E., Graham, G.E., Huston, D.L., Kelley, K.D., Czarnota, K., Paradis, S., Peter, J.M., Hayward, N., Barlow, M., Emsbo, P., Coyan, J., San Juan, C.A., and Gadd, M.G., 2022. Data-driven prospectivity modelling of sediment-hosted Zn-Pb mineral systems and their critical raw materials. *Ore Geology Reviews*, 141, article 104635.
<<https://doi.org/10.1016/j.oregeorev.2021.104635>>

- Lee, C.T.A., and Tang, M., 2020. How to make porphyry copper deposits. *Earth and Planetary Science Letters*, 529, article 115868. <<https://doi.org/10.1016/j.epsl.2019.115868>>
- Lefebvre, D.V., and Jones, L.D., (compilers) 2022. British Columbia Geological Survey mineral deposit profiles, 1995 to 2012; updated with new profiles for VMS, porphyry, and mafic-ultramafic deposits. British Columbia Ministry of Energy, Mines and Low Carbon Innovation, British Columbia Geological Survey GeoFile 2020-11, 652 p.
- Lett, R.E., 2011. Regional Geochemical Survey database 2011. British Columbia Ministry of Energy and Mines, British Columbia Geological Survey GeoFile 2011-07, 2p.
- Lett, R., and Rukhlov, A.S., 2017. A review of analytical methods for regional geochemical survey (RGS) programs in the Canadian Cordillera. In: Ferbey, T., Plouffe, A., and Hickin, A.S., (Eds.), *Indicator Minerals in Till and Stream Sediments of the Canadian Cordillera*. Geological Association of Canada Special Paper Volume 50, and Mineralogical Association of Canada Topics in Mineral Sciences Volume 47, pp. 53-108.
- Logan, J., and Schroeter, T.G., (Eds.), 2013. *Porphyry systems of central and southern BC: Prince George to Princeton*. Society of Economic Geologists Field Trip Guidebook Series 44, 143p.
- Logan, J.M. and Mihalynuk, M.G., 2014. Tectonic Controls on Early Mesozoic Paired Alkaline Porphyry Deposit Belts (Cu-Au Ag-Pt-Pd-Mo) Within the Canadian Cordillera. *Economic Geology*, 109, 827–858.
- Lydon, J. W., 1984. Volcanogenic massive sulphide deposits part 1: A descriptive model. *Geoscience Canada*, 11, 195-202.
- Lydon, J. W., 1988. Volcanogenic massive sulphide deposits part 2: Genetic models. *Geoscience Canada*, 15, 43-65.
- Magoon, L.B., and Dow, W.G., 1994. The petroleum system. In: Magoon, L.B., and Dow, W.G., (Eds.), *The Petroleum System: From Source to Trap*. American Association of Petroleum Geologists Memoir, 60, pp. 2-24.
- McCafferty, A.E., San Juan, C.A., Lawley, C.J.M., Graham, G.E., Gadd, M.G., Huston, D.L., Kelley, K.D., Paradis, S., Peter, J.M., and Czarnota, K., 2023. National-scale geophysical, geologic, and mineral resource data and grids for the United States, Canada, and Australia: Data in support of the tri-national Critical Minerals Mapping Initiative. U.S. Geological Survey data release. <<https://doi.org/10.5066/P970GDD5>>
- McCuaig, T.C., Beresford, S., and Hronsky, J., 2010. Translating the mineral systems approach into an effective exploration targeting system. *Ore Geology Reviews*, 38, 128-138.
- Mudd, G.M., Jowitt, S.M., and Werner, T.T., 2017. The world's by-product and critical metal resources part I: Uncertainties, current reporting practices, implications and grounds for optimism. *Ore Geology Reviews*, 86, 924-938. <<https://doi.org/10.1016/j.oregeorev.2016.05.001>>
- Naldrett, A.J., 1999. World-class Ni-Cu-PGE deposits: key factors in their genesis. *Mineralium Deposita*, 34, 227-240.
- Naldrett, A.J., 2010. Secular variation of magmatic sulfide deposits and their source magmas. *Economic Geology*, 105, 669-688.
- Nelson, J., and Kyba, J., 2014. Structural and stratigraphic control of porphyry and related mineralization in the Treaty Glacier – KSM – Brucejack – Stewart trend of western Stikinia. In: *Geological Fieldwork 2013*, British Columbia Ministry of Energy and Mines, British Columbia Geological Survey Paper 2014-1, pp. 111-140.
- Nelson, J.L. and van Straaten, B., 2020. Recurrent syn- to post-subduction mineralization along deep crustal corridors in the Iskut-Stewart-Kitsault region of western Stikinia, northwestern British Columbia. In: Sharman, E.R., Lang, J.R., and Chapman, J.B., (Eds.), *Porphyry Deposits of the Northwestern Cordillera of North America: A 25-Year Update*. Canadian Institute of Mining and Metallurgy Special Volume 57, pp. 194-211.
- Nelson, J.L., Colpron, M., and Israel, S., 2013. The Cordillera of British Columbia, Yukon, and Alaska: Tectonics and metallogeny. In: Colpron, M., Bissig, T., Rusk, B.G., and Thompson, J.F.H., (Eds.), *Tectonics, Metallogeny, and Discovery—the North American Cordillera and Similar Accretionary Settings*. Society of Economic Geologists Special Publication 17, pp. 53-110.
- Nixon, G.T., Scheel, J.E., Scoates, J.S., Friedman, R.M., Wall, C.J., Gabites, J., and Jackson-Brown, S., 2019. Syn-accretionary multistage assembly of an Early Jurassic Alaskan-type intrusion in the Canadian Cordillera: U-Pb and ⁴⁰Ar/³⁹Ar geochronology of the Turnagain ultramafic-mafic intrusive complex, Yukon-Tanana terrane. *Canadian Journal of Earth Sciences*, 57, 575-600. <<https://doi.org/10.1139/cjes-2019-0121>>
- Nixon, G.T., Scoates, J.S., Milidragovic, D., Nott, J., Moerhuis, N., Ver Hoeve, T.J., Manor, M.J., and Kjarsgaard, I.M., 2020. Convergent margin Ni-Cu-PGE-Cr ore systems: U-Pb petrochronology and environments of Cu-PGE vs. Cr-PGE mineralization in Alaskan-type intrusions. In: Bleeker, W., Houlé, M.G., (Eds.), *Targeted Geoscience Initiative 5: Advances in the understanding of Canadian Ni-Cu-PGE and Cr ore systems—Examples from the Midcontinent Rift, the Circum-Superior Belt, the Archean Superior Province, and Cordilleran Alaskan-type intrusions*. Geological Survey of Canada Open File 8722, pp. 197-218. <<https://doi.org/10.4095/326897>>
- Northcote, B., 2022. Volcanogenic massive sulphide (VMS) deposits in British Columbia: A review. British Columbia Ministry of Energy, Mines and Low Carbon Innovation, British Columbia Geological Survey, GeoFile 2022-11, 30 p.
- Nott, J., Milidragovic, D., Nixon, G.T., and Scoates, J.S., 2020. New geological investigations of the Early Jurassic Polaris ultramafic-mafic Alaskan-type intrusion, north-central British Columbia. In: *Geological Fieldwork 2019*, British Columbia Ministry of Energy, Mines and Petroleum Resources, British Columbia Geological Survey Paper 2020-01, pp. 59-76.
- NRCan, 2020a. Canada-gravity compilation. <<https://open.canada.ca/data/en/dataset/5a4e46fe-3e52-57ce-9335-832b5e79fccc>> Last accessed December 16, 2023.
- NRCan, 2020b. Canada-aeromagnetic survey data compilation. <<https://open.canada.ca/data/en/dataset/752fe3fc-d871-5ae1-9bd9-2b6f65880a8d>> Last accessed December 16, 2023.
- NRCan, 2022. The Canadian critical minerals strategy. Natural Resources Canada, 52 p. <<https://www.canada.ca/en/campaign/critical-minerals-in-canada/canadian-critical-minerals-strategy.html>>
- Nykanen, V., Groves, D.I., Ojala, V.J., and Gardoll, S.J., 2008. Combined conceptual/empirical prospectivity mapping for orogenic gold in the northern Fennoscandian Shield, Finland. *Australian Journal of Earth Sciences*, 55, 39-59.
- Nykanen, V., Törmänen, T., and Niiranen, T., 2023. Cobalt prospectivity using a conceptual fuzzy logic overlay method enhanced with the mineral systems approach. *Natural Resources Research*, 32, 2387-2416. <<https://doi.org/10.1007/s11053-023-10255-8%3e>>
- Ootes, L., 2023. Did epithermal mineralization in the northern Toadogone region develop synchronously with largescale folding? In: *Geological Fieldwork 2022*, British Columbia

- Ministry of Energy, Mines and Low Carbon Innovation, British Columbia Geological Survey Paper 2023-01, pp. 13-21.
- Ootes, L., Bergen, A.L., Milidragovic, D., and Jones, G.O., 2020. Preliminary geology of the northern Hogen batholith and its surroundings, north-central British Columbia. British Columbia Ministry of Energy, Mines and Petroleum Resources, British Columbia Geological Survey Open File 2020-02, 1:50,000 scale..
- Park, J.W., Campbell, I.H., Chiaradia, M., Hao, H., and Lee, C.-T., 2021. Crustal magmatic controls on the formation of porphyry copper deposits. *Nature Reviews Earth and Environment* 2, pp. 542-557.
<<https://doi.org/10.1038/s43017-021-00182-8>>.
- Partington, G., 2010. Developing models using GIS to assess geological and economic risk: an example from VMS copper gold mineral exploration in Oman, *Ore Geology Reviews*, 38-3, 197-207.
<<https://doi.org/10.1016/j.oregeorev.2010.02.002>>
- Piercey, S.J., 2015. A semipermeable interface model for the genesis of seafloor replacement-type volcanogenic massive sulfide (VMS) deposits. *Economic Geology*, 110, 1655-1660.
- Porwal, A., Carranza, E.J.M., and Hale, M., 2003. Knowledge driven and data-driven fuzzy models for predictive mineral potential mapping. *Natural Resources Research*, 12, 1-25.
<<https://doi.org/10.1023/A:1022693220894>>
- Porwal, K., and Kreuzer, O., 2010. Introduction to the special issue: mineral prospectivity analysis and quantitative resource estimation. *Ore Geology Reviews*, 38-3, 121-127.
- Piercey, S., 2011. The setting, style, and role of magmatism in the formation of volcanogenic massive sulfide deposits. *Mineralium Deposita*, 46, pp. 449-471.
- Rees, C., Riedell, K.B., Proffett, J.M., Macpherson, J., Robertson, S., 2015. The Red Chris porphyry copper-gold deposit, Canada: Igneous phases, alteration, and controls on mineralization. *Economic Geology*, 110, 57-888.
<<https://doi.org/10.2113/econgeo.110.4.857>>
- Rezeau, H., and Jagoutz, O., 2020. The importance of H₂O in arc magmas for the formation of porphyry Cu deposits. *Ore Geology Reviews*, 126, article 103744.
<<https://doi.org/10.1016/j.oregeorev.2020.103744>>
- Ross, P.-S. and Mercier-Langevin, P., 2014. The volcanic setting of VMS and SMS deposits: A review. *Geoscience Canada*, 41, 365-377.
<<https://doi.org/10.12789/geocanj.2014.41.045>>
- Samek, W. and Müller, K.-R., 2019. Towards explainable artificial intelligence. In: Samek, W., Montavon, G., Vedaldi, A., Hans, L. K., Muller K (Eds). *Explainable AI: Interpreting, explaining, and visualizing deep learning, state-of-the-art-survey*. Springer, pp. 5-22.
- Sharman, E.R., Land, J.R., and Chapman, J.B., (Eds), 2020. *Porphyry deposits of the northwestern Cordillera of North America: A 25-year update*. Canadian Institute of Mining, Metallurgy and Petroleum Special Volume 57, 726 p.
- Sillitoe, R. H., 1972. A plate tectonic model for the origin of porphyry copper deposits. *Economic Geology*, 67, 184-197.
- Sillitoe, R. H., 2010. Porphyry copper systems. *Economic Geology*, 105, pp. 3-41.
- Singer, D.A., 1993. Basic concepts in three-part quantitative assessments of undiscovered mineral resources. *Natural Resources Research*, 2, 69-81.
<<https://doi.org/10.1007/BF02272804>>
- Singer, D.A., and Kouda, R., 1999. A comparison of the weights-of-evidence method and probabilistic neural networks. *Natural Resources Research*, 8, 287-298.
<<https://doi.org/10.1023/A:1021606417010>>
- Sutherland Brown, A., 1998. *British Columbia's Geological Surveys: A century of science and dedication*. British Columbia Ministry of Employment and Investment, British Columbia Geological Survey Miscellaneous Publication 77 and Pacific Section Geological Association of Canada, 157 p.
- van Straaten, B.I., Friedman, R.M., and Camacho, A., 2023. Stratigraphy of the Stuhini Group (Upper Triassic) in the Galore Creek area, northwestern British Columbia. In: *Geological Fieldwork 2022*, British Columbia Ministry of Energy, Mines and Low Carbon Innovation, British Columbia Geological Survey Paper 2023-01, pp. 33-49.
- Wang, Z., Li, M.Y.H., Liu, Z.-R.R., and Zhou, M.-F., 2021. Scandium: Ore deposits, the pivotal role of magmatic enrichment and future exploration. *Ore Geology Reviews*, 128, article 103906.
<<https://doi.org/10.1016/j.oregeorev.2020.103906>>
- Wearmouth, C., Czertowicz, T., Peters, K.J., and Orovan, E., 2024a. Preliminary mineral potential maps for the porphyry, volcanic massive sulphide, and magmatic mafic-ultramafic mineral systems, northwestern British Columbia. British Columbia Ministry of Energy, Mines and Low Carbon Innovation, British Columbia Geological Survey Open File 2024-05, 1:800,000 scale.
- Wearmouth, C.D., Peters, K.J., Czertowicz, T.A., and Orovan, E.A., 2024b. Mineral potential modelling results for northwestern British Columbia, a comparison between past and current work at the British Columbia Geological Survey. In: *Geological Fieldwork 2023*, British Columbia Ministry of Energy, Mines and Low Carbon Innovation, British Columbia Geological Survey Paper 2024-01, pp. 79-95.
- Wearmouth, C., Czertowicz, T.A., Peters, K.J., 2024c. Preliminary mineral potential maps for the SEDEX and MVT mineral systems, northeastern British Columbia. British Columbia Ministry of Energy, Mines and Low Carbon Innovation, British Columbia Geological Survey Open File 2024-011, 1:500,000 scale.
- Wyborn, L.A.I., Heinrich, C.A., and Jaques, A.L., 1994. Australian Proterozoic mineral systems: essential ingredients and mappable criteria. *Proceedings Australian institute of mining and metallurgy annual conference*. Melbourne, pp. 109-115.
- Yousefi, M., Kreuzer, O.P., Nykänen, V., and Hronsky, J.M.A., 2019. Exploration information systems-A proposal for the future use of GIS in mineral exploration targeting. *Ore Geology Reviews*, 111, article 103005.
<<https://doi.org/10.1016/j.oregeorev.2019.103005>>
- Yousefi, M., Carranza, E.J.M., Kreuzer, O.P., Nykänen, V., Hronsky, J.M.A., and Mihalasky, M.J., 2021. Data analysis methods for prospectivity modelling as applied to mineral exploration targeting: State-of-the-art and outlook. *Journal of Geochemical Exploration*, 229, article 106839.
<<https://doi.org/10.1016/j.gexplo.2021.106839>>



Ministry of
Energy, Mines and
Low Carbon Innovation

